ANNUAL REVIEWS

Annual Review of Biomedical Engineering

Fluid Dynamics of Respiratory Infectious Diseases

Lydia Bourouiba

The Fluid Dynamics of Disease Transmission Laboratory, Massachusetts Institute of Technology, Cambridge, Massachusetts 02139, USA; email: lbouro@mit.edu

Annu. Rev. Biomed. Eng. 2021. 23:547–77

The *Annual Review of Biomedical Engineering* is online at bioeng.annualreviews.org

https://doi.org/10.1146/annurev-bioeng-111820-025044

Keywords

host-to-host transmission, infectious diseases, masks, ventilation, aerosols, airborne, social distancing, multiphase flows, turbulence, fragmentation, COVID-19

Abstract

The host-to-host transmission of respiratory infectious diseases is fundamentally enabled by the interaction of pathogens with a variety of fluids (gas or liquid) that shape pathogen encapsulation and emission, transport and persistence in the environment, and new host invasion and infection. Deciphering the mechanisms and fluid properties that govern and promote these steps of pathogen transmission will enable better risk assessment and infection control strategies, and may reveal previously underappreciated ways in which the pathogens might actually adapt to or manipulate the physical and chemical characteristics of these carrier fluids to benefit their own transmission. In this article, I review our current understanding of the mechanisms shaping the fluid dynamics of respiratory infectious diseases.

Contents

1. INTRODUCTION

As of June 2021, the number of people who have tested positive for severe acute respiratory syndrome coronavirus 2 (SARS-CoV-2) surpassed 179 million worldwide, and the global death toll attributed to the associated coronavirus disease 2019 (COVID-19) exceeded 3.8 million (1). Since the first reported human SARS-CoV-2 infections in late 2019, COVID-19 has placed unprecedented pressure on national health care delivery systems and the global economy. Vaccines are among the most successful public health tools in human history; however, they are not always highly effective (2) or immediately available, particularly for new pathogens such as SARS-CoV-2, or available at all, even for well-known ones such as adult tuberculosis (TB). Even when available, eradication or deployment to maximize population protection takes planning and care and is not always straightforward (3). Therefore, COVID-19 continues to affect the daily life of the general public in unprecedented ways, including the need for increased hand hygiene, regular surface decontamination, social (i.e., physical) distancing, self-quarantine/isolation, and wearing of masks in public, as well as complete or partial closure of entire sectors of the economy, education, and care for the most vulnerable—all in an effort to curb the rapid spread of the virus while the world awaits the widespread availability and distribution of an effective vaccine.

Although it took a global pandemic to make such infection control strategies part of the collective consciousness, respiratory infectious disease outbreaks and epidemics have occurred with some regularity. Within the past 20 years alone, the original SARS affected 26 countries (4), major outbreaks of the Middle East respiratory syndrome (MERS) occurred in 2015 (in South Korea) and 2018 (in Saudi Arabia) (5), spillover of highly pathogenic H5N1 occurred in 2003 (105), and in 2009 an outbreak of the novel influenza A (H1N1) virus originated in the United States

MUCOSALIVARY FLUID

Mucosalivary fluid (MS) is composed mostly of water (99.5%) and a mixture of proteins (0.3%) and inorganic and trace substances (0.2%). Proteins include high-molecular-weight mucins (e.g., MUC5B, MUC7, MUC16) that render the fluid viscoelastic. The rheological properties of MS are important for basic vital functions ranging from ingestion to breathing and innate immunity (11–14).

and developed into a pandemic (6). Regular viral infections include those caused by rhinoviruses, which are nonenveloped and known to be more persistent in the environment than enveloped viruses. Enveloped respiratory viruses include respiratory syncytial virus and parainfluenza and influenza viruses. The envelopes typically involve lipids and glycoproteins that play a role in cell infection of the upper or lower airways. Notably, however, few modern infectious diseases rival TB in transmissibility and impact on human society. Claiming more than one million lives each year (7), TB is the leading cause of death due to an infectious disease worldwide and a leading cause of death due to a curable disease, with a disproportionately greater burden on the least-developed regions of the world (8, 9). With an additional 500,000 lives lost annually to seasonal influenza (10), it seems that, for the foreseeable future, life with respiratory precautions will be the new normal for many. But how do respiratory infectious diseases spread from one host to the next?

Respiratory pathogens are encapsulated within mucosalivary fluid (MS), which breaks, or fragments, into droplets both within and outside of the respiratory tract (RT) (see the sidebars titled Mucosalivary Fluid and Respiratory Tract). The droplets are emitted into the ambient environment within a warm and moist cloud of exhaled air. Such air is emitted at various rates, with volume and momentum depending on the type of exhalation, ranging from regular tidal breathing to panting, speaking, laughing, singing, yelling, coughing, and sneezing. The emitted droplets may be inhaled by a new host, settle in the vicinity of an infected person and contaminate surfaces, or be carried by the exhalation cloud over distances spanning a room. They may evaporate in the ambient environment, leaving behind droplet residues light enough to stay suspended in the air for hours. Such residues might be inhaled by a potential host, be rehydrated in the RT, and then deliver their pathogenic payload deep within the respiratory system to the pathogen's target tissue. All these events involve the interaction of the pathogen with fluid phases—the MS, the warm and moist exhaled cloud, the air of the ambient environment, and the local air–fluid interface and liquid environment of the new host's respiratory system. Understanding host-to-host transmission of respiratory infectious diseases therefore requires understanding the interaction of the pathogen with, and the evolution of, the various fluid phases it encounters. These interactions shape the key physical phases of host-to-host transmission (see figure 1 of Reference 17).

Host-to-host transmission is an obligatory evolutionary phase of respiratory pathogens and is rich in biophysical processes that remain poorly understood. This review synthesizes our current

RESPIRATORY TRACT

The respiratory tract (RT) spans 23 generations of branching airways. The upper RT includes the nasal passage and oropharynx and extends to the trachea (~2 cm diameter) down to the bronchioli (sixteenth generation). The lower RT (sixteenth to twenty-third generations) extends down to the alveoli (~300 μm diameter) (15). The Reynolds number varies from $\sim O(2{,}000)$ in the trachea, with an average tidal volume of 500 mL/breath, to $\sim O(10^{-3})$ in alveolar ducts of ~200 μm diameter (16).

Louis Pasteur (1822–1895)

Pioneers of modern bacteriology. Pasteur, a chemist, is credited with the discovery of vaccination and experimental validation of germ theory. Koch, a physician, discovered the pathogens causing anthrax, tuberculosis, and cholera and experimentally validated the concept of infectious disease transmission.

Robert Koch (1843–1910)

Carl Flügge (1847–1923)

A leader in the science of hygiene, Flügge established an exhaustive body of science on air-, water-, and dust-mediated routes of disease transmission. His seminal work established the importance of respiratory emissions of all types for the transmission of respiratory pathogens.

William Wells (1887–1963)

Wells pioneered the physics-based dichotomized view of respiratory disease transmission via large versus small droplets (aerosols) based on settling versus evaporation timescales. These ideas still underpin the WHO and CDC classification and risk management guidelines for respiratory infectious diseases.

Charles Chapin (1856–1941) Alexander Langmuir (1910–1993)

Chapin, a leading US public health officer, and Langmuir, a prominent figure in the formation of the CDC, fervently opposed the idea of airborne transmission of respiratory diseases, but regretted doing so later in life in the context of measles. Langmuir later admitted the burden of "doctrinal" teaching and called for maintaining the "eternal skepticism of the true scientist" in public health decision-making (Langmuir 1980, p. 40).

Figure 1

Core ideas about germ theory and transmission and their implications for epidemiology and public health, stemming from the legacy of Pasteur, Koch, Snow (not shown), Flügge, and Wells, established modern infection control and epidemiology approaches but were regularly misunderstood, resisted, and dismissed throughout much of history. This is still the case today, as ideas of airborne transmission are often dismissed upon the emergence of new pathogens such as SARS (20) or, more recently, SARS-CoV-2 (21, 22). Abbreviations: CDC, Centers for Disease Control and Prevention; SARS, severe acute respiratory syndrome; SARS-CoV-2, SARS coronavirus 2; WHO, World Health Organization.

understanding of the mechanisms shaping the fluid dynamics of respiratory infectious diseases, with a focus on the transmission processes that are at the core of respiratory infectious disease outbreaks, epidemics, and pandemics such as COVID-19.

2. PENDULUM SWINGS OF TRANSMISSION THEORY: HISTORICAL PERSPECTIVE ON THE ORIGIN OF THE AIRBORNE VERSUS DROPLET ROUTE OF TRANSMISSION DICHOTOMY

The notion that diseases could be contracted through inhalation of so-called bad air dates back millennia and was the foundation of the long-held miasma theory, which posited that epidemics spread through the inhalation of noxious vapors originating from decomposing matter. Not until the mid to late nineteenth century did the germ theory garner scientific support, primarily through a series of definitive experiments by Louis Pasteur (18) and Robert Koch (19), paving the way toward an understanding of the causative agents of disease and to systematic investigations of how contagious diseases spread (**Figure 1**).

In the context of respiratory infectious diseases, at the turn of the last century much interest centered on understanding the host-to-host transmission of TB. The prevailing opinion among physicians at the time was that TB was transmitted mostly through the inhalation of deposited, dried-up tuberculous sputum that is broken up and resuspended in the air in the form of dry dust (23). Today, the dried-out, solid remnants of exhaled mucosalivary droplets are often called aerosols, an umbrella term that denotes any type of matter carried in the air (24). From a fluid dynamic perspective, they are referred to as droplet nuclei or residues, as they are the solid remnants of liquid droplets following desiccation.

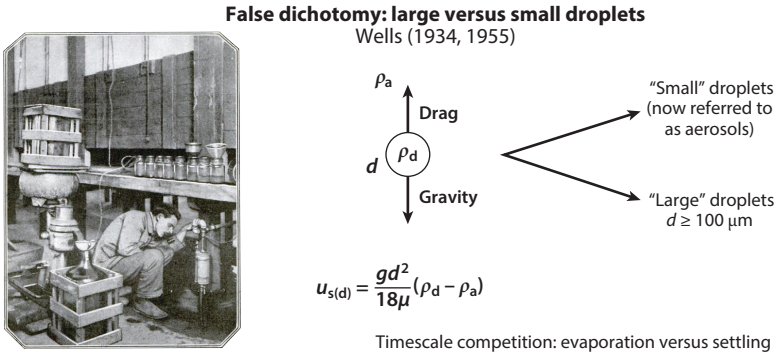

Figure 2

The isolated respiratory drop emission paradigm, which remains the foundation of current infection control guidelines: the dichotomy between isolated small- and large-droplet respiratory emissions (or droplets versus aerosols) (33, 35). The cutoff of 100 μm introduced by Wells relies on a competition between timescales: the settling timescale [from a 2-m height, assuming Stokes settling speed $u_s = (gd^2/18\mu)(\rho_d - \rho_a)$, where g is gravity and ρ_a and μ are the density and dynamic viscosity of the ambient air phase, respectively] and the evaporation timescale (assuming a quiescent ambient and an isolated droplet evaporation model). The model relies on the assumption that respiratory droplets are emitted in isolation (i.e., as a pure liquid spray).

Carl Flügge, then professor of hygiene at the University of Breslau in Germany, challenged this singular focus on airborne transmission via "resuspended dust" and argued that, in infectious diseases of the respiratory system, transmission through contact with liquid mucosalivary droplets emitted by infected individuals presents a much greater risk of infection (23, 25–27). Over a decade, Flügge and his assistants conducted a series of systematic laboratory and clinical investigations into the host-to-host transmission of TB via exhaled droplets, recognizing such notions as evaporation, settling time, infectious dose, and the role of background airflows in dispersing exhaled droplets (25, 27–31). Importantly here, and contrary to today's nomenclature of droplets versus aerosols, Flügge termed all respiratory emissions "droplets," irrespective of their size and final state (liquid droplet or droplet residue/aerosol), as long as they were not yet deposited. In these experiments, collection was done hours after emission, allowing ample settling to occur and not differentiating between liquid and dried droplets. They established that such emissions can easily travel several meters from coughing or sneezing subjects and that it is generally possible to demonstrate the infectivity of the emissions captured at various distances from the patients.

While the extensive work by the Flügge school established a nuanced understanding of respiratory infectious disease transmission in TB, it was soon erroneously reduced to the notion that only ballistic (large) droplet emissions that remain in the liquid state are the major route of respiratory infectious disease transmission. This dramatic reduction changed the view of respiratory infectious disease transmission from the airborne dry resuspended dust route to that of ballistic liquid droplet infection (32, 33).

This view remained unchallenged for 30 years, until William Wells started to examine TB transmission with a focus on the fate of isolated droplet emissions (33–35). On the basis of the droplet diameters, he dichotomized respiratory droplets as large versus small (or droplets versus aerosols), using a 100-μm-diameter cutoff between large and small (**Figure 2**). In his framework, isolated large droplets settle faster than they evaporate and hence fall to the ground within a few seconds, whereupon they contaminate surfaces, typically close to a patient. Small isolated droplets, in contrast, evaporate faster than they settle and form droplet nuclei. Without ambient flow, high

air resistance (drag) prevents isolated small droplets from reaching further than a few centimeters, even if emitted at high speed. Even though it was underpinned by a sound mechanistic model of isolated droplet evolution in the ambient environment, Wells's unified view of TB transmission faced significant opposition and resistance from the medical and epidemiology establishment (36) (**Figure 1**).

One of Wells's chief opponents, Charles Chapin, was an influential public health officer who forcefully defended the view that communicable respiratory diseases are spread by close contact or through indirect contact via droplet transmission (32). Broader failure to recognize the possibility of airborne transmission of diseases such as measles was later attributed, at least in part, to the failure of the leading epidemiologists of the time to question the prevailing doctrines and to conduct conclusive field studies that may have settled the issue for a variety of infectious diseases (32). Therefore, doctrine prevailed over scientific method. Despite such resistance, however, Wells persisted and eventually prevailed. Aided by supporting evidence from a series of systematic and careful laboratory experiments, Wells's physics-based dichotomy of respiratory infectious disease transmission was eventually accepted and is still at the core of World Health Organization (WHO) and Centers for Disease Control and Prevention (CDC) classification schemes (37, 38), albeit with a default focus on the droplet route for most respiratory diseases, even in the absence of confirmatory evidence in the time of emerging pathogens, such as SARS-CoV-2.

Today's classification schemes employ various arbitrary diameter cutoffs, from 5 to 10 μm, to classify host-to-host transmission into droplet versus aerosol routes on the basis of the inhalation potential of such drops. Consequently, infection control strategies have been built around the dichotomy between a large-droplet route, with a focus on droplet precautions and surface contamination, and an aerosol route, with a focus on high-grade respirators. Not surprisingly, in the event of an emerging respiratory infectious disease outbreak, as was the case with SARS-CoV and now SARS-CoV-2, public health officials have become interested in droplet size distributions to determine which route dominates and which precautions should be mandated. However, the problem with this dichotomy, as we now know, is that it is false.

3. SHIFT IN PARADIGM: FROM RESPIRATORY ISOLATED DROPLETS TO THE TURBULENT MULTIPHASE CLOUD

While physically elegant, Wells's isolated droplet model does not capture a central physical characteristic of exhalations. Exhalations do not eject isolated MS droplets into the environment. Exhalations—ranging from speaking to yelling, coughing, and sneezing—are made up of a turbulent multiphase cloud whose physical properties have significant implications for the range and longevity of the ejected mucosalivary droplets and, hence, for their fate, their range of contamination in space and time, and associated risk-assessment and risk-mitigation strategies (17, 21, 39–41). The turbulent exhalation cloud consists of warm and moist exhaled air laden with mucosalivary droplets ranging in size from $O(1\ \mu m)$ to $O(1\ mm)$ (39). The locally warm and moist atmosphere within the exhaled cloud protects the smaller droplets from immediate evaporation, and its momentum carries them forward much farther (by a factor of more than ~200 for drops below 10 μm) than they would be able to travel were they emitted in isolation (21, 39, 40). Importantly, the range of all droplets is extended, and contrary to the Wells picture, the smallest droplets tend to travel the farthest (21, 39) (**Figure 3*a***). In fact, it is not the size of the droplets at emission that determines their range but rather the characteristics of the warm and moist gas cloud that is emitted and carries them forward. Only after the emitted cloud slows down sufficiently do droplet and residue sizes become important determinants of dispersal in background low-velocity indoor airflows (a few centimeters per second) and penetration of the respiratory system.

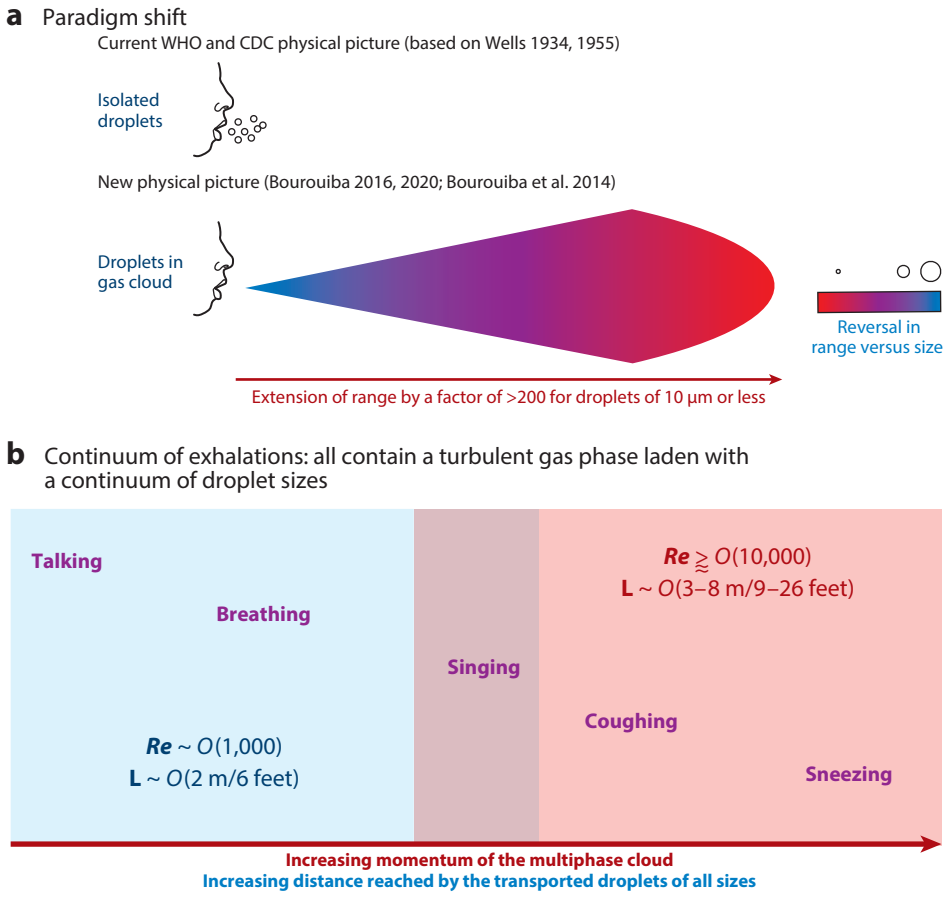

Figure 3

(*a*) Paradigm shift from Wells's isolated droplet picture to that of the high-momentum turbulent (high-*Re*) multiphase exhalation cloud that carries droplets much further than if they were emitted in isolation (by a factor of at least 200 for drops <10 μm). Moreover, the smaller drops are carried over macroscopically important distances in a few seconds, even in the complete absence of background ventilation flow. The physical picture of respiratory multiphase cloud emission (**Figure 4**) applies to a range of exhalations, as long as the key assumptions of the point-source emission and sufficiently high *Re* are satisfied to ensure turbulence of the cloud. (*b*) These assumptions remain valid for breathing as well as for more violent exhalations such as coughing and sneezing, as was recently confirmed in experiments on speech and high-fidelity numerical simulations of violent exhalations (42, 43). Abbreviations: CDC, Centers for Disease Control and Prevention; *Re*, Reynolds number; WHO, World Health Organization.

3.1. The Respiratory Exhaled Cloud Governs the Range of Air and Surface Contamination

From a fluid dynamic perspective, the respiratory cloud emission is a discrete emission of mass and momentum that undergoes two phases: (*a*) an initial continuous jet phase that is brief compared with the subsequent evolution of the cloud and (*b*) a longer-lasting puff phase. Both jets and puffs are momentum-driven turbulent bodies of fluid ejected from a point source (here, the mouth). Along their trajectory $s(t)$, the lateral dimension $r(t)$ of the jet and puff [measured orthogonal to $s(t)$] grows as $r(t) = \alpha s(t)$, where α is a (constant) entrainment coefficient, due to lateral momentum diffusion and edge eddies entraining quiescent ambient air (17, 39) (**Figure 4*a*,*b***).

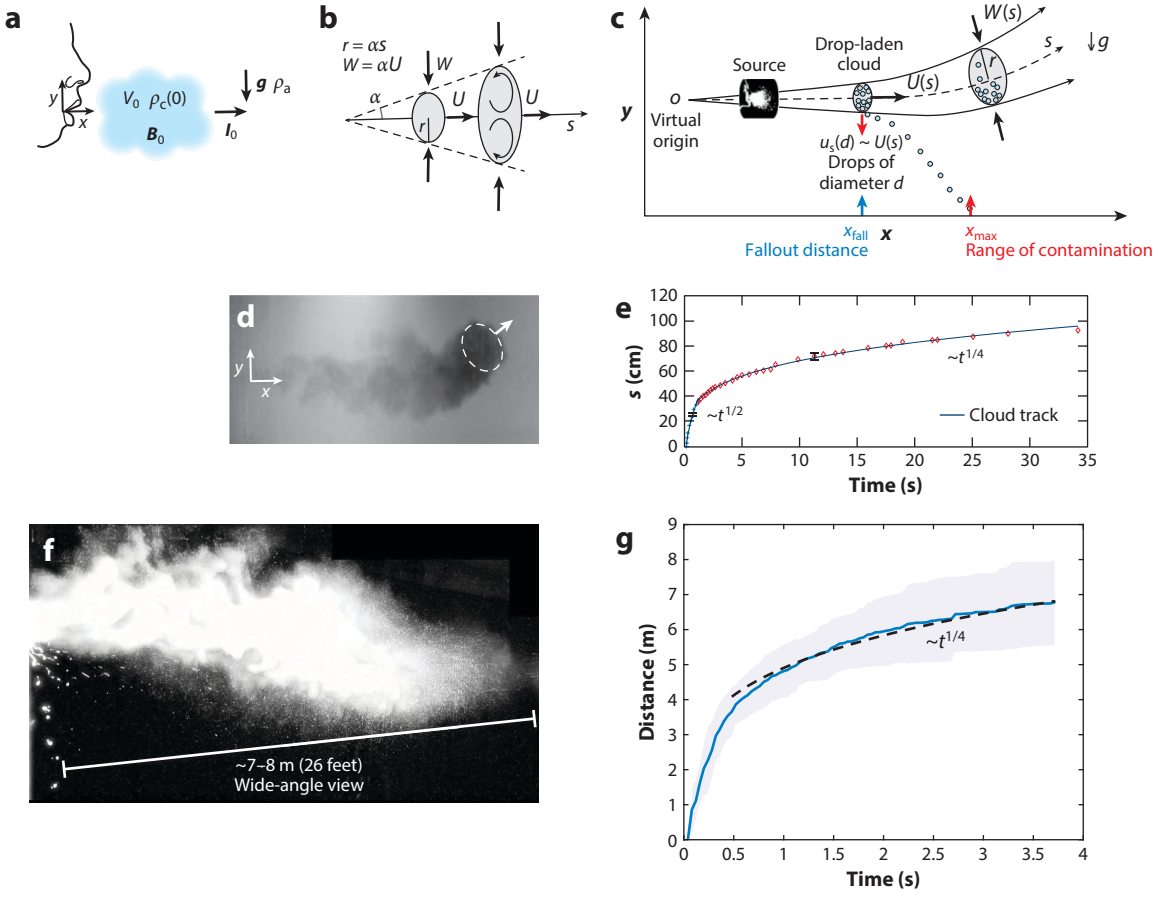

Figure 4

(*a*) Exhaled air with initial volume V_0 and momentum I_0 containing mucosalivary droplets of a given size distribution forms the multiphase cloud of initial density $\rho_c(0)$ and initial buoyancy B_0. (*b*,*c*) The turbulent point-source emission evolves according to a self-similar growth with a signature conical shape along its curvilinear trajectory (s, θ). The mean velocity of entrainment from the edges of the cloud, W, is proportional to the mean forward velocity of the cloud, $U(s)$; in other words, $W(s) = \alpha U(s)$, where α is the entrainment coefficient. The dynamics of the cloud and the fate of its droplet payload are modeled using a continuous settling model, enabling the prediction of the entire trajectory of the cloud, as well as the ranges over which droplets of a given size leave the cloud and how far away they would settle on surfaces or remain suspended. This model has been validated in both (*d*,*e*) analog experiments and (*f*,*g*) human exhalations. These findings reveal the importance of accounting for the cloud's multiphase turbulent puff nature, as the characteristic scaling evolution of $s \sim t^{1/4}$ is robustly demonstrated (39). The cloud dramatically extends the distance reached by the droplets, even in the absence of ambient airflow or ventilation, enabling the smaller drops to travel up to 8 m in a few seconds in a concentrated manner rather than being well mixed in indoor spaces. The implications are important for evaluation of risk and contamination and for infectious disease guidelines (e.g., **Figure 5**) (21, 41).

Assuming discrete momentum-dominated emissions, the initial jet-like phase is characterized by conservation of momentum flux, $M_0 \sim \rho_c r^2 (ds/dt)^2$, where ρ_c is the density of the multiphase cloud, throughout the brief, continuous emission process (150–200 ms for a sneeze and 200–300 ms for a cough). Combining the conservation of momentum flux with the self-similar growth of the cloud's lateral dimension, $s \sim r$, leads to the scaling law $s \sim t^{1/2}$ for the initial temporal evolution of the gas cloud (17, 39). Subsequent to the emission period, momentum is no longer continuously injected; rather, it is conserved. This is the longer-lasting puff phase. The

conservation of initial momentum $I_0 \sim \rho_c r^3 (ds/dt)$, when combined with the self-similar growth of the cloud, leads to the scaling law $s \sim t^{1/4}$ during the puff phase (17, 39). These scaling laws are concrete predictions of the turbulent multiphase cloud model that derive from the entrainment closure of the governing equations (39, 44), a surprisingly robust characteristic of such point-source turbulent clouds across applications ranging from geophysical and industrial systems (45) to exhalations (**Figure 4*e*,*g***). The $t^{1/2}$ and $t^{1/4}$ scaling-law predictions have been experimentally verified in physical analog experiments, in human sneezes and coughs (21, 39) (**Figure 4*d–g***), and, more recently, in high-fidelity numerical simulations of violent exhalations (43) and further human exhalation experiments such as speech (42) and additional violent exhalations (E. Villermaux & L. Bourouiba, original data) (**Figure 4*g***). When exhalations are performed in rapid succession, a continuous emission closer to the limit of a jet with $s \sim t^{1/2}$ is recovered for a time (42).

The motion of an exhalation cloud is well captured by a point-source multiphase turbulent puff physical picture (39). An isolated mass of turbulent gas laden with liquid drops moves through a quiescent environment with an average speed $U(s)$ along its curvilinear trajectory, at first driven by its initial and discrete momentum, with a possible role for buoyancy depending on ambient conditions. Assuming an initial momentum I_0 and initial buoyancy B_0, a one-phase cloud of density ρ_c, suspended droplet number N, cloud volume V, buoyancy B, and momentum I, one can show that the cloud's evolution is governed by

$$\frac{dN}{dt} = -\frac{3U_s N}{2\alpha s}, \quad 1.$$

$$\frac{dV}{dt} = 3\eta\alpha^3 s^2 \frac{ds}{dt} + v_p \frac{dN}{dt}, \quad 2.$$

$$\frac{d\rho_c}{dt} = \frac{1}{V}\left[v_p \frac{dN}{dt}(\rho_p - \rho_c) + 3\eta\alpha^3 s^2 \frac{ds}{dt}(\rho_a - \rho_c) \right], \quad 3.$$

$$\frac{dB}{dt} = g\rho_a \frac{dV}{dt} - g\frac{d(V\rho_c)}{dt}, \quad 4.$$

$$\frac{dI_y}{dt} = B, \quad 5.$$

$$\frac{ds}{dt} = \sqrt{I_y^2 + (I_0 \cos\theta_0)^2}/(V\rho_c), \quad 6.$$

where η is a shape parameter that reflects the ellipsoidal shape of the cloud (39, 45), v_p is the volume of the (here monodisperse) droplets in the cloud, ρ_a is the density of the ambient air, θ_0 is the initial angle of the trajectory $s(t)$ measured with respect to the horizontal direction, and g is gravitational acceleration (39). In this validated model, the speed of the cloud decreases as ambient quiescent air is entrained into the cloud. Droplets of size d continuously settle out of the cloud when their speed, $U_s(d)$, exceeds the continuously decreasing mean forward speed of the cloud, $U(s)$ (39) (**Figure 4*c***). The resultant model is closed in the sense that it does not contain any free parameters that need to be fitted: It is predictive from initial conditions. The system of Equations 1–6 is valid for exhalations ranging from tidal breathing to coughing and sneezing and can be used to predict contamination as a function of distance and time since emission (L. Cooper, C. Lu & L. Bourouiba, original data).

The turbulent cloud model predicts that the smallest droplets go the farthest. Rather than encountering significant air resistance, limiting their motion to a few centimeters in the absence of ambient airflow, droplets are instead carried forward by the momentum of the turbulent cloud (39), extending the range of droplet emissions up to 7–8 m for sneezes (21, 39, 40). This is in contrast

to the view to which Flügge's extensive work had been reduced, namely that ballistic large-droplet emissions set the range of contamination to a maximum of 1–2 m from a cougher/sneezer (**Figure 3*a***) in the absence of background airflows. Interestingly, the long range of such droplet emissions during coughs and sneezes had already been observed in the 1890s by von Weismayr (46) and Laschtschenko (29) despite their relatively limited understanding of the fluid dynamics involved. They rinsed the mouths of healthy volunteers with a saline suspension of *Bacillus prodigiosus* (*Serratia marcescens*) and had the subjects speak naturally at various intensity levels, cough, and sneeze. They showed that colonies grew in petri dishes positioned as far as 185 cm from the speakers, 4 m from the coughers, and 9 m from the sneezers (29, 46).

Reynolds number (*Re*): inertial force divided by viscous forces: $Re = Q/\nu d_m$, where Q is the volume flow rate, ν is the kinematic viscosity, and d_m is a characteristic length. *Re* is 600–800 for breathing and $O(10^4)$ for coughing/sneezing, spanning the turbulent regime from breathing to talking, singing, coughing, and sneezing, in order of increasing momentum

3.2. The Cloud and Its Intermittency Change Droplet Evaporation

The warm and moist local cloud environment and the cloud's turbulent intermittency delay droplet evaporation in the moving multiphase cloud, by a factor of up to 1,000 (21), compared with evaporation of isolated droplets, with significant implications for pathogen persistence. Recent high-fidelity numerical simulations of respiratory point-source emissions estimated a delay in evaporation by a factor of at least 30 in standard indoor conditions, due to the cloud's sheltering effect on its droplet payload (43).

Given the success of the validated turbulent cloud model in explaining and predicting the fluid dynamics of respiratory emission events, it has become obvious that the current paradigm of respiratory infectious disease transmission, still based on Wells's dichotomized picture of isolated large versus small/aerosol droplet emissions (**Figure 2**), needs to be abandoned or reframed to incorporate the underlying physics of air versus surface spatiotemporal dynamics of contamination. Accordingly, the WHO and CDC risk and infection control guidelines need to be updated in favor of a paradigm that incorporates the notion of a continuum of droplet sizes and the more nuanced and accurate physics of fluids governing their dynamics, range, and evaporation, thus determining risks of contamination in space and time, patterns of transmission, and respiratory protection needs in a variety of natural and built environments.

4. THE MULTIPHASE TURBULENT CLOUD MEETS AMBIENT AIRFLOWS

As the exhaled multiphase turbulent puff cloud advances upon emission (**Figure 4**), its forward speed decreases as it grows through entrainment of quiescent ambient air. After sufficient time elapses, the forward speed of the cloud becomes comparable to the comparatively low [O(1–10 cm/s)] background air speed naturally found indoors. When this occurs, the droplets and droplet nuclei that remain trapped in the cloud and carried forward over O(10 m) for the most violent exhalations (21, 40) may settle if their settling speed is greater than the ambient ventilation airflow. Otherwise, they are advected by the background airflow and disperse, rather than remaining concentrated in a coherent cloud moving forward.

Under well-mixed indoor conditions, average ambient airflow is $\lesssim$25 cm/s in the occupied zone of the room. It is largely determined by the specifics of the indoor ventilation (e.g., mechanical, natural, displacement, or mixing ventilation) and the geometry of the space, though additional factors can also affect indoor airflow. Human occupants and electric devices produce heat, inducing plumes that contribute to the overall airflow, on average and instantaneously, leading to peak velocities of O(10 cm/s) and up to 600 L/min in the vicinity of a person in otherwise-still ambient conditions of average temperature (~20°C) (47). However, these airflows do not account for the momentum-driven exhalations directing exhaled flow horizontally toward others. Normal

tidal breathing alone can generate the turbulent multiphase jets discussed above, with a Reynolds number (*Re*) of ∼600–800, that can easily reach distances on the order of 1–2 m (**Figure 3**).

Upon slowdown of the respiratory cloud and the balance between its mean velocity and the background airflow in an indoor space, the remaining suspended droplets and droplet nuclei disperse via background turbulence. Such dispersal can be estimated using classical Richardson's law for relative dispersal in a turbulent flow (48, 49): $\delta_{\mathrm{Ri}}(t) = At^{\beta/2}$, where $\beta = 3$ and $\delta_{\mathrm{Ri}}(t)$ is the root-mean-square separation between two particles (here, droplets or their residues). The constant A is the product of the Richardson constant and the turbulent dissipation rate per unit mass, which itself is a function of the intensity of the ventilation imposed in the space. The root-mean-square distance between droplets then evolves as $\delta_{\mathrm{Ri}}(t) \sim t^{\beta/2}$, assuming the flow is statistically steady.

We therefore have two regimes: (*a*) early respiratory emission governed by the dynamics of the respiratory point-source turbulent puff cloud entrainment described in Section 3, during which the cloud's speed continuously decreases as it entrains ambient air (**Figure 4**), and (*b*) cloud dispersal via turbulent background flow. At a transition time t_*, the cloud's growth via entrainment, $\dot{r}(t) \sim t^{-3/4}$, becomes negligible compared with its dispersal via background turbulence, $\dot{\delta}_{\mathrm{Ri}}(t) \sim t^{(\beta-2)/2}$. The transition time t_* between regimes is obtained by balancing these two growth/dilution rates: $\dot{\delta}_{\mathrm{Ri}}(t_*) = At_*^{(\beta-2)/2} = \dot{r}(t_*) = Bt_*^{-3/4}$. The prefactors A and B account for the specifics of the turbulence and sources. Note that $\beta = 3$ from Richardson's dispersal theory (48), but it is an upper estimate of the power law of $\delta_{\mathrm{Ri}}(t)$. Instead, experimental studies support lower values for the $\delta_{\mathrm{Ri}}(t)$ power law (50). Experimental observations in quiescent ambient suggest a transition time t_* from a few dozen seconds to minutes, depending on indoor conditions, type of respiratory emission, and initial source emission momentum I_0 (**Figure 4**; Section 3).

4.1. People–Air–Surface–Space Integrated Infection Control Management: Early and Late Regimes for Pathogen Dispersal and Persistence

Both the pre- and post-t_* regimes are important to determine indoor exposure risk and to plan for an integrated people–air–surface–space (PASS) (41) management strategy of transmission risk mitigation (**Figure 5*b*,*c***). The early regime is that of the respiratory cloud evolution. Although relatively short, it can evolve rapidly and over long distances and involve exposure to fresh emissions of potentially high pathogen concentration. Additionally, fresh emissions contain pathogens that have a higher probability of being alive and infectious (see Section 5.3 on pathogen persistence). In this cloud evolution regime, the cloud's droplet payload is not diluted homogeneously in the volume of the indoor space but rather remains highly concentrated in the evolving volume of the cloud and is diluted only by entrainment of ambient air, where the cloud volume ($\sim r^3$) scales as $r^3 \sim t^{3/4}$ for $t < t_*$ (puff phase), and then $\sim t^{3\beta/2}$, where $\beta \lesssim 3$ for $t > t_*$ (the abovementioned Richardson turbulence dispersal). During the puff phase, exposure from inhalation is also governed by the settling of droplets/nuclei over time. The settling of droplets on surfaces leads to a reduction of risk from inhalation and is governed by the competition between the puff cloud's average velocity and the settling speed of the droplets/particles determining their fallout. For this first regime, source control and physical distancing strategies, possibly integrating new designs of local airflows and office spaces, for example, are critical (**Figure 5*c*,*d***). Masks reduce the range of all exhalations (51) (**Figure 5*b***). However, unless the masks are fitted to be sealed, leakage occurs with an emerging cloud that has a reduced momentum (**Figure 5*a***; Section 4.2).

The late regime is that of dispersal by background airflow, which can last for hours to days, depending on the indoor ventilation and its maintenance. Here, dilution is more important than in the first regime, so exposure is eventually reduced if the well-mixed limit of the space is reached.

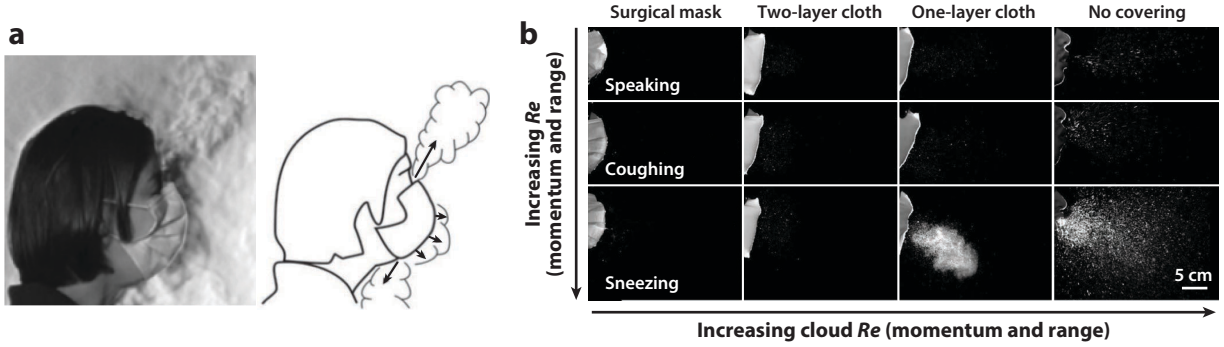

d

Type of activity	Level of group activity: Low occupancy — Outdoors and well ventilated	Low occupancy — Indoors and well ventilated	Low occupancy — Poorly ventilated	High occupancy — Outdoors and well ventilated	High occupancy — Indoors and well ventilated	High occupancy — Poorly ventilated
Wearing face coverings, contact for short time						
Silent						
Speaking						
Shouting, singing						
Wearing face coverings, contact for prolonged time						
Silent						
Speaking		*		*		
Shouting, singing						
No face coverings, contact for short time						
Silent						
Speaking						
Shouting, singing						
No face coverings, contact for prolonged time						
Silent						
Speaking						
Shouting, singing						

Risk of transmission: Low — Medium — High

* Borderline case that is highly dependent on quantitative definitions of distancing, number of individuals, and time of exposure

(*Caption appears on following page*)

Figure 5 (*Figure appears on preceding page*)

Integrated PASS infection control management. (*a*) Masks reduce the forward momentum of the turbulent gas cloud and its droplet payload, though poor seals allow the gas cloud to follow the path of least resistance and partially escape from the unsealed openings. (*b*) Residual droplet emission as a function of type of exhalation and degree of protection. (*c*) PASS concept integrating the source dynamics with the space and environmental conditions that need to be considered for effective infection control over short to long space and timescales. (*d*) Qualitative relative risk determination of SARS-CoV-2 transmission from asymptomatic individuals in different settings and for different occupation times, activities, ventilation, and crowding levels. Abbreviations: CFM, cubic feet per minute; PASS, people–air–surface–space; *Re*, Reynolds number; SARS-CoV-2, severe acute respiratory syndrome coronavirus 2. Panel *a* adapted from Reference 55. Panel *b* adapted from Reference 51. Panel *d* adapted from Reference 41.

However, the well-mixed limit in occupied indoor spaces is rarely reached, and care needs to be taken to ensure that no high-risk zones of accumulation or airflow recirculation exist. Note that airflow patterns and heterogeneity in an indoor space change on the basis of occupancy number and duration, coupled with the type of venting system and its maintenance. In particular, displacement ventilation, in which fresh air is supplied at relatively low velocity close to the floor and extracted near the ceiling, is known to have energetic advantages as well as advantages in terms of its ability to maintain a fresh breathing zone. It does require sufficiently high ceilings to ensure the development of a transition layer that separates the contaminated upper stratum from the lower fresh air region (52), in addition to ensuring that such a transition layer be sufficiently high and stable to perturbations, such as opening a door or window or connecting to another room (52, 53). When mechanical ventilation is not optimal, natural ventilation can remarkably increase the dilution level in an indoor space: Open windows can lead to 20 air changes per hour (ACH). For comparison, indoor spaces with optimized mechanical ventilation can typically reach 10 ACH (54).

Air changes are important to estimate with respect to occupancy: A crowded space requires more air changes than a nearly empty one. Thus, the minimum injection of clean air per person is an important additional metric—O(7–10 L/s per person) is recommended (54)—although it was established in the context of odor and temperature comfort. In the context of respiratory pathogen transmission, such as *Mycobacterium tuberculosis*, a minimum of O(15 L/s per person) is needed to reduce the attack rate (56).

It is also important to avoid recirculation of untreated air whenever possible. If air recirculation is necessary, its decontamination (mechanical filters, chemical or light-driven decontamination) is critical, particularly in a time of pandemic. Finally, when leveraging natural ventilation to optimize air changes, it is important to not neglect the potential to mitigate risk during the early-time regime of exhalations. Although opening of windows and doors in a classroom can dramatically increase the ACH on average (tackling the late regime of dispersal), it remains important to maintain nonoverlapping breathing zones of the occupants and avoid ending up extending, via directional persistent flow patterns, the breathing zone of one occupant into the inhalation zone of another, even if masks are in use. Rather than focusing only on wearing masks or on engaging in physical distancing, an integrated PASS approach to indoor risk mitigation must take into consideration the occupants' activities (e.g., speaking versus exercise), crowding, ventilation type and capacity per person, and decontamination of both air and surfaces to assess and mitigate relative transmission risk (**Figure 5**).

Attack rate: ratio of new cases to the number of exposed individuals during a fixed-duration event where transmission could have occurred, here involving sharing of an indoor space

4.2. Source Control and Inhalation Protection: Face Coverings

While the use of personal protective equipment of various gradations (e.g., surgical masks or N95 or P100 respirators) is common practice, and even mandated in certain clinical environments during certain procedures and amid pandemics, one of the most passionately discussed topics

outside of Asia is the use of face masks by the general public. In that context, masks aim to serve two purposes: to trap the pathogen-bearing droplets of an infected individual (source control) (21) and to protect individuals wearing masks by filtering pathogens in the air. Various studies have shown that the use of masks for source control and protection may help limit airborne transmission (57–60).

Compared with cloth masks or medical/surgical masks, high-grade P100 or N95 respirators typically offer greater protection. A mask's filtration efficiency (FE) is a key metric that quantifies its protective capacity. FE is calculated as $FE = 1 - C_D/C_U$, where C_U and C_D are the upstream and downstream number densities of particles per volume of air, respectively; C_D/C_U is also referred to as the penetration. FE depends on the tightness of the material's weave, fiber or thread diameter, and, in the case of nonwoven materials, the manufacturing process. FE is also a function of the particle diameter and flow rate used to challenge the tested material, not accounting for the fit of the mask on the face. The fit factor (FF, or fit) is the ratio of concentration into and out of the mask, accounting for both the FE and seal of the mask. In contrast to penetration, FF is measured when a user is wearing the mask (**Figure 5*a*,*b***). For a mask to be maximally effective, a tight seal is needed.

High FE of a given material is achieved by combining mechanical and electrostatic filtration approaches, typically Brownian motion, inertial impaction, and electrostatic forces for particle interception and capture. Interception via Brownian motion is effective for small particles below 30 nm, while inertial impaction is more effective for larger particles above the micrometer scale, resulting in a nadir in FE for particles between 100 nm and 1 μm (61). Regarding mechanical interception, the increase in filtration is associated with a pressure drop across the mask; therefore, a resistance to breathing and a consequent compromise between FE and breathability are required. Charging the material enhances filtration without further pressure drop. Thus, procedures that degrade the charge should be avoided, raising key questions about the efficacy of the mask after various procedures of decontamination or prolonged usage. Indeed, increased humidity, for example, may affect filter charge. Data collected in various humidities with varying airflows are conflicting (62–65).

Previous studies reported FE for cotton-based fabrics ranging from 10% to 60% when tested with particles between 20 nm and 1,000 nm in diameter and with an airflow speed of 5.5 cm/s (66). Some materials had slightly decreased FE when the velocity was increased to 16.5 cm/s (66). A more recent study showed that FE for other cotton-based fabrics ranged between 9% and 96% for particles <300 nm and, similarly, between 14% and 99.5% for particles >300 nm with a flow rate of 1.2 $feet^3$/min (0.03 m^3/min) (67). This wide range of reported FE values shows the importance of not substituting physical distancing with masks. Both should be used under a comprehensive PASS integrated infection control strategy (**Figure 5*b*,*c***; Section 4.1). Additionally, the current fabric testing paradigm addresses only filtration of particulate matter or droplets, ignoring the effects of the high-momentum turbulent gas cloud from violent exhalations. Indeed, the intensity of exhalation combined with filtration and face seal determines the reduction of momentum and load of particles exhaled in the cloud that escape sideways, posing a residual risk to bystanders (**Figure 5*a***). There remains limited information on respirators' extended use, reuse, and decontamination. For decontamination, certain methods are promising, but further research for validation is needed. The methodologies for testing filtration and persistence of biological agents on masks are not standardized, leading to contradictory results; consequently, it remains difficult to compare the efficacy of decontamination approaches. Understanding the properties of the inhaled particles is an important first step, discussed in the next section (L. Cooper & L. Bourouiba, original data).

5. THE DROPLETS IN THE RESPIRATORY CLOUD

5.1. Respiratory Droplet Size Distributions and Emission Load: Variability and Need for Standardized Measurements

Motivated by Wells's isolated droplet–versus–aerosol dichotomy (**Figure 2**), many studies aimed to determine the sizes and numbers of droplets emitted from breathing, talking, singing, coughing, and sneezing. **Figure 6*a*** shows such distributions in the form of size probability density functions (PDFs). Droplets range from submicrometer to millimeter sizes. No single instrument can capture this full size range. Moreover, the variation in instrumentation between studies, or even within one study when combining different instruments, requires scrutiny. When normalizing each PDF by its own average diameter (**Figure 6*b***), a more consistent picture of single-mode distributions per instrument type with comparable standard deviations emerges. The few multimode outlier distributions are attributable to the composite instrumentation. Clearly a more fundamental understanding of the composite mechanisms that govern the fragmentation of MS into droplets is required to clarify the bounds of validity variable distributions (Section 5.2).

We separated the reported data according to emission type and instrumentation used (**Figure 7**). According to the information found in each study, we used or computed the concentration for each emission. First, it is clear that coughs received much more attention than all other types of emission. Second, the variability in reported concentrations is huge, spanning orders of magnitude [$O(1) - O(10^5)$ particles/cm^3] for coughs, for example. The instrumentation and methods used to measure such particle sizes and concentrations range from interferometric Mie imaging to laser diffraction or single-particle scattering [aerodynamic particle sizing (APS), optical particle counting or sizing (OPC or OPS)] (94–96), electric mobility [scanning mobility particle sizing (SMPS)], inertial or electric low-pressure impaction (cascade and cyclone impactors), and droplet deposition, as well as impaction and manual or automatic counting from slides via imaging.

The instrumentation, calibrations, and tolerance to background noise (background particle load in the air) associated with these approaches vary widely and require a priori assumptions about optical properties of the droplets or particles; their evaporation rates; impact and contact line dynamics (for impaction); hygroscopic properties when condensation is required for counting (e.g., SMPS); and density, shape, sphericity, and compactness (for electric mobility). These properties are particularly difficult to infer for droplets made of complex, heterogeneous biological fluids or compounds (see Section 5.2). Thus, the measurements vary in sensitivity and precision across the size spectrum, and some of these modalities have only a narrow measurement range, are not necessarily calibrated to a common reference, and may only read out data sequentially across size bins, rendering the measured distributions highly dependent on sampling duration (97). These problems are particularly acute when the sampled flow of interest is a transient impulse, such as an exhalation. Additionally, droplet sizes tend to be determined only at a single location (typically away from the source), which poses a basic undersampling problem in space and time. The high variability between the settings of one instrument and between instruments as well as nonstandardized protocols about location of measurement and environmental conditions make it difficult to compare distributions and reconstruct concentrations across studies (**Figures 6** and **7**). Measurements of droplet sizes are also particularly challenging because of the dynamic nature of the droplets, which change over time following emission; their complex, heterogeneous biological composition, which is typically unknown; and the fact that the multiphase puff cloud, and its payload of droplets, is itself dilute, moves very quickly and transiently, and is spatially and temporally intermittent due to its turbulent flow nature. Thus, it is critical to exercise caution in reducing methodological variability that confounds the measurements and not to overinterpret the features of these distributions.

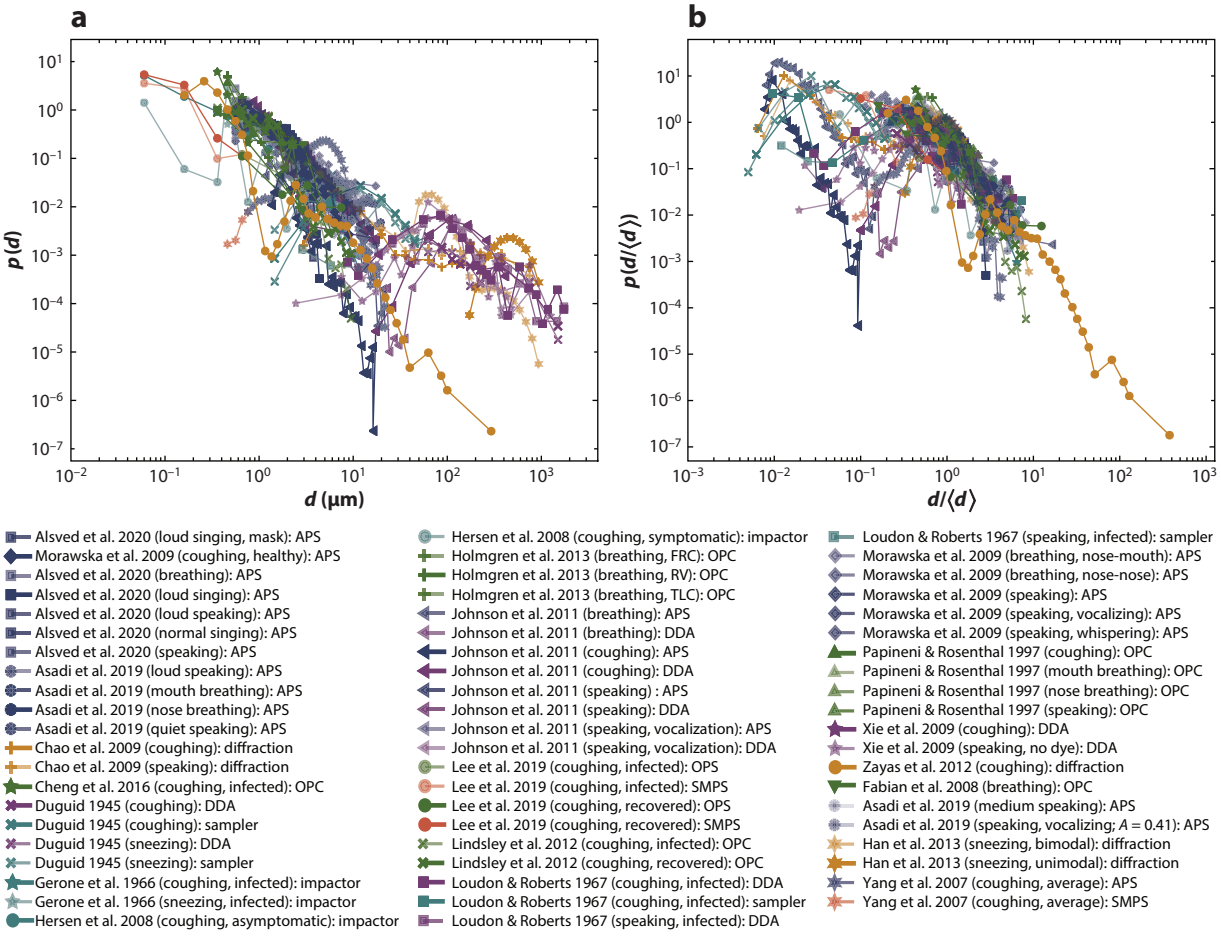

Figure 6

(*a*) Droplet size distributions from the literature (69–93) comparing respiratory emissions under a range of conditions; measured with different instrumentation and at different distances from the mouth from breathing (nose and mouth), speaking, coughing, and sneezing; and examining both infected and healthy subjects. The range of instrumentation used to capture these distributions varies widely between studies (see **Figure 7**). In some cases, in single studies, instruments are combined to allow a range from a few millimeters to a few micrometers to be captured. (*b*) When normalized by the mean diameter of each distribution, the graphs mostly collapse on a unified curve shape for the same instrument, but variability remains. For example, one study (92) combined impaction and aerodynamic particle sizing, with a gap in resolution of drop size in the 10-μm transition region (L. Cooper, C. Lu & L. Bourouiba, original data). Abbreviations: APS, aerodynamic particle sizer; DDA, droplet deposition analysis; FRC, functional residual capacity; OPC, optical particle counter; OPS, optical particle spectrometer; RV, residual volume; SMPS, scanning mobility particle sizer; TLC, total lung capacity.

The choice of instrumentation clearly has a first-order effect on the range of sizes reported, to the point that the differences in reported concentrations and distributions between studies overpower the differences in range and concentration of emission from one respiratory event to another, or in emission from a healthy versus infected patient, within a single study. Therefore, it is necessary to standardize such experiments and have a standard of reporting so as to ensure comparison and integration of the data reported in the field. Indeed, we found that many studies

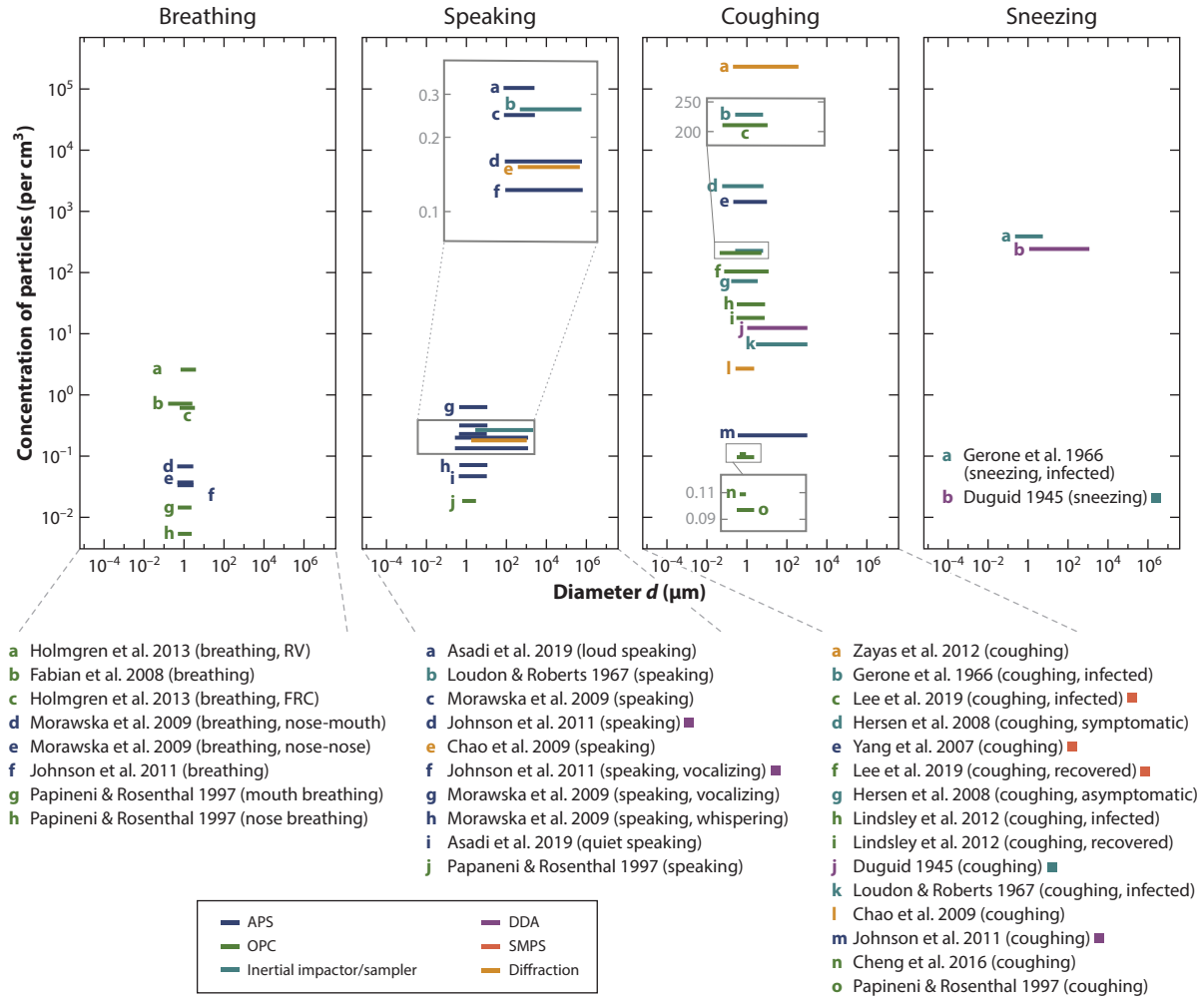

Figure 7

Compilation of results from the literature on quantification of droplet concentrations in a range of respiratory emissions from both infected and healthy subjects, showing a wide range of variation in instrumentation used (*color key*) (69, 76–79, 83–86, 89–93). The studies that combined instruments are marked with a square in the color corresponding to the other instrument used. Clearly, cough measurements dominated earlier research, while comparatively little attention has been paid to other emissions. However, even for coughs, the concentration of exhaled droplets varies between studies by orders of magnitude. Further analysis of the data from **Figure 6** reveals that the variability between studies is greater than the variability between emission events within a study (e.g., studies comparing a cough and a sneeze with the same setups), making it difficult—without further detailed analyses of experimental conditions and parameters of measurements, which, surprisingly, are not always reported in full—to compare studies and draw conclusions regarding the robustness or validity of reported concentrations, amounts, and size ranges of drops emitted for a particular respiratory maneuver (e.g., sneeze versus cough) or between healthy and infected subjects (L. Cooper, C. Lu & L. Bourouiba, original data). Abbreviations: APS, aerodynamic particle sizer; DDA, droplet deposition analysis; FRC, functional residual capacity; OPC, optical particle counter; RV, residual volume; SMPS, scanning mobility particle sizer.

do not provide sufficient information to infer concentration or emission per unit of time. The lack of standardization in publications, in addition to the lack of consistency in protocols or instrumentation settings, hinders the ability to gain insight into the dynamics and variability of respiratory emissions across studies. Examples of missing information that could allow one to compare results

in the literature are prevailing humidity and temperature during sampling at various locations, duration of measurement and distance from source, total volume of air sampled, and number of exhalations used for a measurement.

Refinement of measurement techniques and standardization of how such measurements are performed with indirect methods would gain from being complemented by a mechanistic understanding of how droplets form within and outside the RT. Indeed, such a fundamental understanding could enable us to derive physically based expected physiological bounds on the range of mucosalivary droplet sizes and speeds and their distributions. Such a mechanistic understanding could also enable us to establish or rule out hypotheses about droplet formation and allow for advances in diagnostics and risk assessment based on the biomechanics and underlying physics of the complex, multiscale, unsteady fluid fragmentation governing such processes (discussed in the next section).

Weber number (*We*): ratio of kinetic to surface energy, $We = \rho v^2 d/\sigma$, of a fluid with density ρ, characteristic velocity v, characteristic length d, and surface tension σ

Ohnesorge number (*Oh*): relative magnitude of viscous to inertial and surface tension forces: $Oh = \mu/\sqrt{\rho\sigma d} = \sqrt{We}/Re$, where μ is the fluid's dynamic viscosity

Deborah number (*De*): ratio of relaxation time λ to capillary time τ: $De = \lambda/\tau$

Capillary time (τ): $\tau = \sqrt{\rho d^3/\sigma}$

5.2. Fluid Fragmentation and Mechanisms of Selection of Droplet Sizes and Loads: Coupling of Unsteady Flow and Complex Fluid

Violent exhalations are a vital defense mechanism complementing mucociliary clearance. They can be triggered by an increase in mucus secretion, inflammation, ciliary dysfunction, or subtle mechanisms deriving from infection that also benefit the dissemination of the pathogens involved (98–100). The size and speed distributions as well as pathogen concentration of the droplets generated and emitted in the exhalation process govern the transport, persistence, and infectivity of the pathogen payload. Respiratory pathogens surely adapted to this obligatory phase of host-to-host transmission so as to maintain the cycle of infection on which their survival depends. In order to clarify the origin of the physiological difference among individuals and their ability to transmit, it is crucial to decipher the physics driving the amount, composition, and pathogen load of the droplets emitted, coupled with the multiphase physics of the cloud and its momentum, in various exhalation events.

What generates the MS droplets (see the sidebar titled Mucosalivary Fluid for composition) and the cloud that transports them also determines the range and footprint of contamination. Such generation mechanisms are inherently a physical process of fluid fragmentation: the breakup of fluid from bulk into spray. Such fragmentation occurs when shearing, stretching, or otherwise induced thinning forces imposed on a bulk fluid overcome surface tension and viscous forces (101, 102). The former tend to promote fluid breakup, while the latter tend to dissipate imparted energy and so mitigate fragmentation. Surface tension and viscous forces also tend to minimize a fluid's surface area; therefore, higher surface tension and fluid viscosity generally favor formation of larger droplets, while higher air speeds impacting on or shearing a fluid surface tend to favor generation of smaller droplets. More specifically, the hydrodynamic instabilities governing the creation of droplets range from shear driven to capillary driven, with more complex versions of classical instabilities such as the Kelvin–Helmholtz, Rayleigh–Plateau, and Rayleigh–Taylor instabilities (103). The regimes of such fragmentation processes are described by the Weber number (*We*), which quantifies the competition between kinetic and surface energy. When *We* is high, kinetic energy dominates over surface energy, and fragmentation of a bulk fluid into droplets is favored (101, 104). Other nondimensional numbers relevant to fragmentation are the Ohnesorge (*Oh*) and Deborah (*De*) numbers, which quantify the effects of viscosity and elasticity, respectively, compared with capillary effects. The timescales relevant for these instabilities include the relaxation time (λ), which, for polymeric fluids such as MS under stretching, is the average time needed for polymers to relax to their equilibrium configuration. Th capillary time (τ) characterizes, at first order, the breakup timescale of Newtonian low viscosity fluids.

The fragmentation of bulk respiratory fluid is a multiscale process, analogous to—though more complex than—the fragmentation processes reported in other industrial or environmental systems (17, 101, 103). The complexity of respiratory fluid fragmentation derives primarily from the facts that (*a*) the exhalation flow from breathing to coughing or sneezing is inherently unsteady and transient; (*b*) the geometry and physiology of the RT (see the sidebar titled Respiratory Tract for dimensions and scales) are multiscale, with branching, curved, and compliant airways giving rise to rich nonlinear biomechanical and biofluidic phenomena (16, 106); and (*c*) the liquid phase is a complex viscous or viscoelastic biofluid. Thus, the product of the respiratory fluid fragmentation process is governed by the time-varying dynamics of destabilization as well as by the fluid properties (e.g., Newtonian versus non-Newtonian) (107, 108). The physicochemical and biological attributes of the fluid phase are therefore important, as are the (highly transient) flow profiles: There is a rapid flow rate increase and then a slow decrease in the course of an exhalation, the relative period of each phase varying in timescale and volume depending on the type of exhalation (see, e.g., **Figure 8** for coughs). We expect inherent variability in droplet production and exhalation contamination footprint between individuals, due to differences in airflow capacity, rheology of the respiratory liquid lining in various regions of the RT, and health status. Yet these properties have historically been poorly characterized (with recent progress discussed in the next sections).

5.2.1. Unsteady exhalation flow. As mentioned above, the respiratory fragmentation and corresponding emission processes are brief: Droplet emission from exhalation flows lasts 100–200 ms for sneezes and 200–300 ms for coughs (39, 109) and is driven by a rapidly increasing then slowly decreasing transient airflow (see, e.g., **Figure 8*l*** for coughs). Such short-lived, unsteady fluid fragmentation processes confer on the droplets time-varying characteristics that are important determinants of risk of contamination and, hence, for controlling the chain of transmission (17, 108). In contrast, for steady fragmentation (101, 110–112) the properties of the generated spray droplets are independent of time or are all formed at the same time. Unsteady fragmentation typically occurs by transforming a fluid bulk into a sheet followed by ligaments and then droplets via a series of surface tension–dominated instabilities (103, 108, 113). In the RT, these include mechanisms of (*a*) film burst, such as bubble or clogging-bag burst, leading to secondary droplet formation from film rupture and destabilization into ligaments and droplets (114–117) (e.g., **Figure 8*a*,*b*,*d***), or (*b*) fluid shearing by time-varying airflow profile (e.g., **Figure 8*l***), giving rise to a more complex version of the Kelvin–Helmholtz instability, which, in turn, eventually leads to emission of ligaments and droplets as well (104).

In fact, these processes are also directly observable in respiratory fluid fragmentation, as the fluid breakup process is not confined to the RT. The sequence of images in **Figure 8*a–c*** shows how bulk MS emitted at the mouth is stretched, over the course of less than 5 ms, to form films that rupture to form ligaments and droplets. The droplets formed, here outside of the RT, are superposed on those formed at various locations within the RT (109). **Figure 8*b*** shows more clearly the sheet formation that eventually ruptures (**Figure 8*c***), leading to a rim formation due to the pull of surface tension. Similar to bag burst in jets and cross-flows (116), bubble formation and bursting are also observed in respiratory emissions (**Figure 8*d***). These mechanisms share the fragmentation mechanics of bubble bursts and complex and contaminated thin-film ruptures (114–116, 118, 119). Key determinants of these mechanisms are the fluid composition, including surfactant levels and impurities, which here would be in the form of cells or inhomogeneous distributions of clumps of polymers. The location in the RT determines in large part the composition and hence the rheological properties (discussed further in Section 5.2.3).

5.2.2. Multiscale nature of the respiratory tract. The local *We*, *Re*, and *Oh* values within the RT, coupled with fluid properties, local geometry, and compliance of the RT walls, determine the

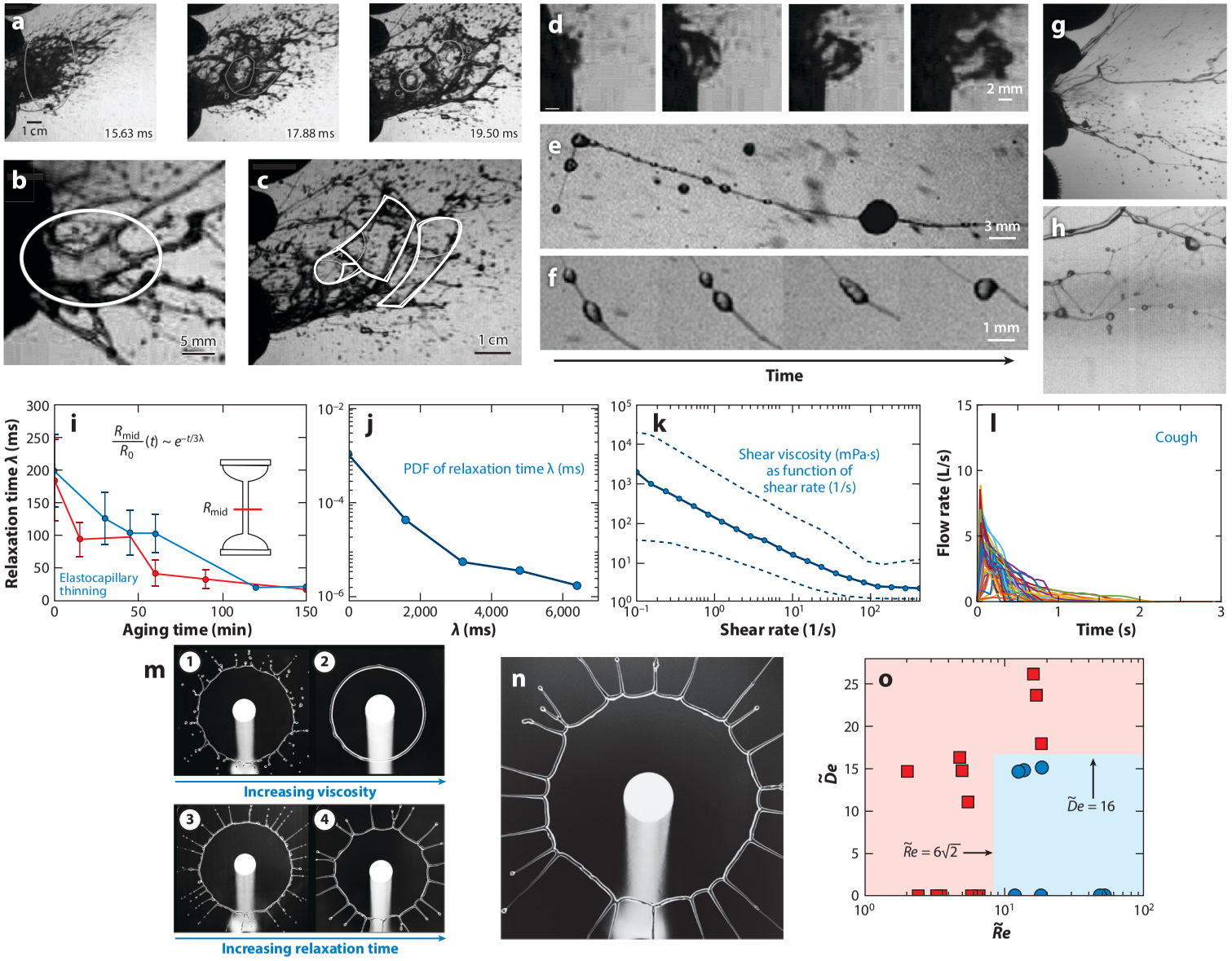

(Caption appears on following page)

Figure 8 (*Figure appears on preceding page*)

(*a*) Sequence of emission of mucosalivary fluid (MS) from the respiratory tract (RT) during violent exhalations. The bulk of MS transforms into sheets that pierce with fluid retraction into ligaments. (*b*) Sheet formation. (*c*) Film rupture, upon which rims form. (*d*) Bubble or bag bursting inside or outside the RT also generates respiratory droplets. (*e*) Ligaments from viscoelastic fluids can persist longer under extension than their Newtonian inviscid counterpart, with beads on a string and (*f*) merger and gobbling over 13 ms. (*g*) The role of viscoelasticity in human exhalation (*b*) captured qualitatively by the destabilization of a sheared mimic viscoelastic fluid. (*i*) Relaxation time λ of human MS decreases rapidly over time from collection. (*j*,*k*) Range of values of (*j*) elasticity, with relaxation time probability distribution function (PDF) measured for fresh MS samples, and of (*k*) MS viscosity as a function of shear rate for samples from 72 individuals. (*l*) Fragmentation of MS inside and outside of the RT is driven by an unsteady airflow (N. Bustos & L. Bourouiba, original data). (*m*,*n*) Importance of reduction to a standardized fluid fragmentation process for calibration and validation of respiratory biofluidic mimics. (*m*) Sheet expansion in air upon impact of a droplet on a pole with a size comparable to that of the impacting droplet for fluids of increasing viscosity from (①) $\mu = 4.2$ mPa·s, with $Oh = 0.007$, $Re = 4{,}100$, $De = 0$, and $We = 889$, to (②) $\mu = 14$ mPa·s, with $Oh = 0.024$, $Re = 1{,}300$, $De = 0$, and $We = 930$, and increasing relaxation time from (③) $\lambda = 3.5$ ms and $\mu = 2.5$ mPa·s, with $Oh = 0.0046$, $Re = 6{,}700$, $De = 0.29$, and $We = 1{,}000$, to (④) $\lambda = 5.8$ ms and $\mu = 2.5$ mPa·s, with $Oh = 0.005$, $Re = 6{,}300$, $De = 0.44$, and $We = 1{,}015$, all with capillary times of $\tau \approx 14$–15 ms. (*n*) Fragmentation of MS with similar fluid properties as fluid ④ in panel *m*, showing elongated ligaments and beads on strings of panels *a*, *c*, and *e*–*h*. The rod diameter in panels *m* and *n* is 6 mm, and the droplet diameter is 4.3 mm. (*o*) Regime map in terms of the local rim's $\tilde{Re}$ and $\tilde{De}$. The Newtonian fluid limit of unsteady fragmentation is valid in the blue region, while viscous and elastic effects dominate droplet size selection in the red region (17, 125). Abbreviations: *De*, Deborah number; *Oh*, Ohnesorge number; *Re*, Reynolds number; *We*, Weber number.

dominant local modes of breakup. Droplets can be produced by a range of mechanisms dominated by capillary, inertial, elastic, or viscous and elastocapillary effects depending on the location within the RT. Regarding film formation and burst, the film thickness and lifetime depend on the film's location within the RT and are critically affected by the local fluid composition [e.g., the surfactant and polymeric content determining its rheology (115, 118, 119)]. Such a film arises from MS shearing into film; thick plug formation followed by a burst in the upper airway; or periodic, gentler capillary film formation followed by high rupture speeds inducing effective fragmentation into numerous smaller droplets. The thinner the film is, the higher its rupture speed will be. The idealized case is the static homogeneous film governed by the Culick rupture retraction speed, $v \sim 1/\sqrt{h}$, where h is the film thickness (120). Within the RT, such processes can also be facilitated by airway wall compliance and oscillation enabling plug formation and rupture when the lining of the walls interact. Such airway closure or semiclosure may be responsible for signatures or modes of distributions of droplet sizes superposed on the macroscale droplet sizes generated from shear or bag burst from larger upper-airway plug fragmentation. In addition to affecting the droplet sizes and speeds, the location of droplet formation might influence a droplet's pathogen load, given that some pathogens preferentially invade certain regions of the RT. *M. tuberculosis*, for example, preferentially proliferates and remains dormant in the alveoli, while rhinoviruses preferentially colonize upper RT cells.

Finally, the RT serves as a filter in the selection of the droplets that make it out of the host, and also influences the penetration and deposition of pathogen-laden droplets inhaled by an exposed individual. This filtering capacity arises from the inherent multiscale geometry of the RT and the variation of flow regimes within it, as its curved and branching geometry creates well-known patterns of Dean flow, recirculating and vortical flows (15), and possible impaction points and drop trapping on the way up or down the RT. The combination of these mechanisms (shear or stretching, film or plug burst) of fragmentation, in addition to filtration, can lead to various signatures of drop distributions—associated with different compositions as well—superposed on one another. It is this superposition that would be observed when measuring emissions outside the RT at a single point (e.g., as done in **Figures 6** and **7**). This superposition, coupled with the unsteadiness of the process, makes it more difficult to disentangle the signature of each fragmentation mechanism involved. Indeed, unsteadiness even for simpler configurations of

fragmentation introduces various apparent modes into the droplet distributions, even if the process of fragmentation continues to produce unimodal signatures of drops, though with properties (mean, standard deviation) varying with time (17, 108).

5.2.3. Mucosalivary fluid composition and rheology. The rheology of the fluid lining the RT is important to determine. MS is a dilute polymer solution based on a Newtonian solvent—water—and a range of polymers that provide the fluid with its viscoelastic properties. **Figure 8*a–c*** illustrates the ability of such fluids to form persistent filaments and delay capillary breakup when stretched. Indeed, even in minute amounts, the polymers found in MS can yield dramatic differences in the behavior of the fluid under extension, in comparison to water, due to the increased resistance within extended ligaments to flow. The dynamics observed involve nonlinear effects arising from the finite extensibility of the polymer chains within the fluid. Moreover, under certain flow regimes and when capillary, viscous, and inertial effects balance, additional structures can appear, such as so-called beads on a string (121, 122) (**Figure 8*e–h***). These can evolve to create merger and gobbling effects (109) (**Figure 8*f***). The additional dynamics of viscoelastic stretching in a transient turbulent background flow, ligament persistence prior to drop formation, and beads-on-a-string and gobbling/merger behavior all contribute additional features to the final droplet size distribution—broadening it on the large drop size end—of an exhalation when compared with the distribution from a steady fragmentation process of a Newtonian fluid (123). Similarly, the ligaments are observed to persist at finer scales much longer than water filaments do. **Figure 8*e,f*** shows ligaments with diameters on the order of 0.2 mm. If the fluid were water only, then the associated breakup time would be the capillary timescale of $\tau \approx 330$ μs. Yet the filaments persist as long as 13 ms—40 times longer—owing to the retarding effect of viscoelasticity, here with estimated Oh and De values of $Oh \approx O(10^{-3})$ and $0.65 \leq De \leq 78.73$. This thinning is also associated with the generation of droplets smaller than what would be generated by water ligaments of identical size; therefore, here too, viscoelasticity can broaden the final droplet size distribution, enhancing the relative contribution of the finer droplets. A better understanding and assessment of droplet emissions from respiratory events and their role in transmission of infectious diseases will depend on the characterization of MS rheology at various stages of health and infection.

Despite the obvious importance of MS properties in determining respiratory fragmentation outcome, the rheology of the human respiratory system fluid lining is not well known. Although several recent studies have reported viscosity and elasticity values, they are inconsistent. We attribute such inconsistencies in part to the methodology of sample collection and preservation, sample age at time of measurement, and precision of measurement. These confounding factors are often not reported, making it difficult to interpret the results. In past and ongoing research (N. Bustos & L. Bourouiba, original data), we have characterized the properties of MS secretions in both healthy and influenza- or cold-infected individuals and noted the strong sensitivity of the results to the method of collection and time of measurement of the sample properties (**Figure 8*i–k***). Such measurements are taken via capillary thinning, during which a sample of MS is stretched between two plates to form a liquid bridge—a filament. A laser micrometer or direct optical measurement tracks the midpoint radius of the filament as it thins under the action of capillary forces. Once fluid inertia can be neglected, the filament thinning process is initially governed by a viscocapillary force balance in which viscous extensional stresses oppose the increasing capillary pressure, followed by a later elastocapillary phase in which stresses generated by the stretching of the polymer chains dominate (**Figure 8*i***). From measurements of the time evolution of the filament radius, one can obtain the breakup (i.e., capillary) time of the filament and the relaxation time λ of the fluid via the evolution $R(t)/R(0) \sim e^{-t/3\lambda}$, where $R(t)$ is the diameter of the filament (**Figure 8*i***). Other techniques, such as pendant drop and shear rheometry, provide measurements of surface tension

and shear viscosity. **Figure 8*k*** clearly shows shear-thinning behavior for MS, though in the regime relevant for human exhalations, the viscosity is close to (albeit a little higher than) that of water.

Finally, what is clear from our study is that MS properties are delicate to characterize, as rapid degradation of elastic properties due to sedimentation and clumping of the polymeric content makes the samples inhomogeneous and watery over the first hour (**Figure 8*i***). It is also critical to be cautious when determining inter- and intrasubject variability in health versus infection, given the wide range of relaxation time values we have observed on the basis of more than 560 independent measurements in more than 70 healthy and infected individuals (N. Bustos & L. Bourouiba, original data) (**Figure 8*j***). Therefore, if researchers do not either slow down sample degradation or rapidly measure the rheological properties during collection, they will obtain erroneous results, which could in part explain the wide and contradictory range of values reported in the literature. In fact, most measurements of relaxation times of MS in the literature do not include the sample age, making it difficult to infer the physiological relevance of the values reported. Finally, now that we have gained some clarity regarding the unsteadiness, rheology, and complexity of the problem, it is crucial to break it down into tractable parts and derive mechanistic insights to determine how each part of this complex multiscale problem contributes to the final spray and emission characteristics. Next, I discuss how insights obtained from a standardized analog canonical fragmentation system that captures some of the essential physical features of transient unsteady fragmentation processes relevant to respiratory emissions can help shed light on the role of the various components of the problem (**Figure 8*m–o***).

Local rim Reynolds number: $\tilde{Re} = v_b b/\nu$, where v_b and b are the rim velocity and thickness as measured in the local noninertial reference frame of the rim

Local rim Deborah number: $\tilde{De} = \lambda/\sqrt{\rho b^3/\sigma}$ in the noninertial frame of the rim of size b

5.2.4. Canonical, axisymmetric unsteady fragmentation. The axisymmetric unsteady fragmentation process resulting from the impact of a droplet on a target of comparable size (**Figure 8*m*,*n***) results in rich, coupled, spatially and temporally varying, multiscale, nonlinear processes that can be broken down into sheet and rim evolution and determination of droplet size and speed distributions (17, 124). Upon impact, the droplet is transformed into a rapidly expanding two-dimensional fluid sheet whose rim continuously destabilizes, generating fluid ligaments that, in turn, destabilize and shed droplets, mostly one at a time throughout the sheet expansion process. Rim destabilization depends on the impacting droplet's *We* and fluid properties: Increasing the viscosity and relaxation time of the surrogate fluid reduces the number of ligaments generated and droplets shed (**Figure 8*m***). Manipulation of these fluid properties results in fragmentation that closely resembles that of fresh human saliva (**Figure 8*n***), showing elongated ligaments and beads on a string reminiscent of those observed via direct imaging of respiratory fluid fragmentation from physiological emission (**Figure 8*a*,*b*,*e–h***).

This canonical fragmentation problem provides fundamental insights regarding when the roles of viscosity and elasticity must be incorporated explicitly and when they can be neglected for their effect on the spray of interest. Indeed, in the Newtonian inviscid limit, the droplet size and speed distributions can be predicted exactly and are given by a superposition of Gaussian distributions with time-varying mean, with smaller and faster droplets shed early in the unsteady process and larger and slower droplets shed later (17, 124). Therefore, the unsteadiness of the fragmentation process inherently causes the observed skewness of the droplet size and speed distributions. The prediction is predicated on the balance of inertial and surface tension forces in the local reference frame of the rim. This criterion holds for complex fluids for which $\tilde{Re} \gtrsim 8$ and $\tilde{De} \lesssim 16$, where $\tilde{Re}$ and $\tilde{De}$ are the *Re* and *De* in the local rim reference frame (**Figure 8*o***). Outside of this region, modifications in the computations of droplet sizes and speeds would be required to account for nonnegligible viscosity and elasticity effects of the MS (**Figure 8*o***).

5.3. Persistence, Exposure, and Infection

In addition to the droplet sizes, it is important to determine whether pathogens are present and infective in the droplets as a function of droplet size and history of emission from the source. This determination depends on the droplet volume sampled, handling procedures, and amplification approaches (126, 127). The persistence of pathogens refers to their ability to remain alive and multiply, successfully penetrate and hijack a target cell in the case of viruses, and multiply within the cell with various degrees of virulence or effectiveness. For most pathogens, we have only a rudimentary understanding of their persistence and the mechanisms shaping it. We know that SARS-CoV-2 remains infective even after 24 h of deposition on cardboard and 2–3 days on stainless steel (128). For comparison, respiratory syncytial virus or influenza can survive on nonporous surfaces for at least 6 h (129). In contrast, rhinoviruses and adenoviruses have been reported to survive for days on nonporous surfaces (130). When airborne, the measles virus was found to maintain its infectious state for at least 1 h (131, 132), while aerosolized *M. tuberculosis* has a half-life of approximately 6 h under controlled (rotating drum) conditions (133). Similarly, aerosolized H3N2 influenza virus remains infective for at least 2 h (134) and aerosolized SARS-CoV-1 for 1 h (128). Recent studies of aerosolized SARS-CoV-2 found viable virus up to 3 h postaerosolization (128, 135) and up to 16 h in suspended aerosols (136).

Despite these reports, major questions remain unresolved regarding the persistence of pathogens in the environment, whether deposited on surfaces or suspended in the air in a dried or semidried state. The composition of the fluid phase, environmental conditions (temperature and humidity), macro flows, microphysics, and fluid dynamics involved at the small or intermediate scale all play a role in determining pathogen survival. In the context of SARS-CoV-2, lower temperatures appear to promote survival (137–139), while the pH of the carrier fluid has a negligible effect (137, 140); however, the influence of humidity on SARS-CoV-2 survival seems to depend on the characteristics of the carrier fluid (135). Clearly, these are still preliminary results. The fluid dynamic, biological, and environmental factors are extremely entangled, and current experimental results and data do not yet allow us to decipher the key underlying mechanisms governing the wide range of results observed. The interplay between the physics and biology of pathogen-bearing droplets in relation to pathogen persistence is very rich, and disentangling these coupled relationships will remain a fascinating problem.

6. DISCUSSION AND PERSPECTIVE

In the context of respiratory diseases, the generation of mucosalivary droplets and their emission as part of a multiphase turbulent gas cloud, coupled to their evolution in the environment through multiphase droplet and phase-change physics of evaporation and condensation, ultimately determine the nature, composition, and size of the droplets or the droplet nuclei/residue inhaled by a potential host. The size and composition of the inhaled particles determine not only the range and evolution (adhesion or resuspension for example) of the nuclei in the environment but also their potential for penetration deep into the RT and, thus, access to preferential target tissue for the pathogens carried. Inoculation of animals suggests that for the same viral load, the inhalation of an atomized solution results in higher infection and death rates in comparison to dry intranasal inoculation (33, 141).

There remain important areas of research to examine, such as deposition and penetration in the context of droplet residues, as a function of the history of the complex biological particles carrying the pathogens of interest. In addition, rich questions regarding the interplay among transmission physics, complex biochemistry, and host immunology remain open. Of special interest regarding this interplay might be the mucous barrier of the upper airways, as it is the first

line of defense against respiratory infectious agents (98). Here, the history of the pathogen-laden droplet (evaporation, desiccation, rehydration) determines, in part, the success of host-cell infiltration and infection. Finally, these questions of persistence are at the crux of transmission in indoor spaces, including nosocomial transmission occurring in (*a*) health care facilities, known to have been critical in the spread of coronaviruses such as MERS (142), and (*b*) mostly households and indoor environments, for SARS-CoV-2.

At the clinical and practical levels, important questions remain pertaining to generation of contaminated droplets from exhalations as well as from procedures such as intubation or high-flow nasal cannula treatment with oxygen and humid air (143). These procedures are also important in mitigating potential transmission to health care workers and patients due to life-saving procedures. Other questions concerning the environment involve the need for a better understanding of the mixing and dispersal of contaminants, for example, from the motion of people in a confined space or from natural or mechanical ventilation, as well as the need to better characterize and innovate in low-cost ventilation technologies able to produce stable stratified environments (e.g., displacement ventilation) with breathing zones that are free of contaminants.

In summary, we need a mechanistic understanding of the interfacial physics, including the rheology of respiratory secretions in health and infection, and the associated complex multiscale and varied mechanisms of fluid fragmentation in a range of configurations, such as unsteady processes typical of respiratory events (17). Such an understanding will be critical for building the foundation required to capture quantitatively, and thus predict, the complex fluid processes governing spray generation in a range of configurations and dynamic regimes during exhalations from healthy and infected individuals. Similarly, understanding such processes will be crucial for deciphering the role of interventions, such as masks and the environment, including ambient moisture and temperature. With regard to moisture, the large-scale epidemic data sets examined to date seem to suggest reduced transmission in the 40–60% range of relative humidity (C. Verheyen & L. Bourouiba, original analysis), though it has also been argued that lower humidity favors rapid droplet evaporation and hence increases air contamination. It has also been argued that SARS-CoV-2 is comparatively fragile and that viruses that dry faster die faster. Yet, laboratory-based controlled aerosolization experiments with SARS-CoV-2 have resulted in somewhat conflicting results. Moreover, the turbulent cloud of human exhalations shields droplets from immediate evaporation. All this suggests that the role of humidity and temperature and their significance in the chain of respiratory disease transmission are still not mechanistically understood; thus, caution in interpreting claims about their effect is needed. Finally, an understanding of the effect of airflow in a health care environment versus an office can help pave the way toward innovations in infection control that can leverage such processes to reduce transmission in common shared spaces.

COVID-19 has brought to the fore the urgent need to understand and mitigate host-to-host transmission during the ongoing global pandemic. However, the need to base our understanding of this obligatory phase of a respiratory pathogen's life cycle on a solid mechanistic understanding has always been urgent and applies equally to the transmission of seasonal influenza, TB, and a wide range of emerging and reemerging respiratory infectious diseases. Such a mechanistic understanding provides the opportunity to predict and control the risk of transmission. It aids in early detection and allows for new pathways for drug discovery tackling the transmission phase. It also allows for mitigation of epidemics in the critical early phase, prior to the availability of effective vaccines or drugs. In the context of respiratory infectious diseases, the fluid dynamics and biophysics of pathogen extraction, emission, persistence, and host invasion and infection (17) give rise to a large set of biomedical, physiological, and complex and multiscale fluid dynamics questions that deserve to be addressed through rigorous and mechanistic approaches combining

novel tools for experimental quantification as well as theoretical and numerical modeling. Finally, it will be crucial to integrate such knowledge in the multifaceted context of testing, tracking, treatment, and vaccination strategies, as well as in creating predictive epidemic models over the months and years to come in order to ensure greater resilience to the inevitable recurring epidemics of respiratory pathogens.

DISCLOSURE STATEMENT

The author is not aware of any affiliations, memberships, funding, or financial holdings that might be perceived as affecting the objectivity of this review.

ACKNOWLEDGMENTS

The work discussed in this review involved discussions, mentoring of students, and collaboration with colleagues with whom it was a pleasure to exchange over the years. In particular, I thank S. Balachandar, James Bales, Emery Brown, John Bush, Nicole Bustos, Lauren Cooper, Anjini Chandra, Eline Dehandschoewercker, Bryan Grenfell, Martha Gray, Ning Guan, Howard Heller, James Hughes, Jeffrey Koseff, Sungkwon Lee, Detlef Lohse, Claire Lu, Raina MacIntyre, Michael Mackey, Taronna Maines, Dimitrios Papavassiliou, Joanna Pulit-Penaloza, Kyu Rhee, Barry Scharfman, Alexandra Techet, Emmanuel Villermaux, Jianhong Wu, and Stéphane Zaleski. The research and discussions were made possible by support in part from the MIT Reed and Edgerton Funds, the Burroughs Wellcome Fund, the Wellcome Trust, the Richard and Susan Smith Family Foundation, William Olbricht at the Multiphase Fluid Dynamics Section of the National Science Foundation, the National Institute for Occupational Safety and Health/Centers for Disease Control and Prevention, Vision Research, TSI, SKC, and Steelcase.

LITERATURE CITED

1. Dong E, Du H, Gardner L. 2020. An interactive web-based dashboard to track COVID-19 in real time. *Lancet Infect. Dis.* 20:533–34
2. Blanton L, Dugan V, Elal A, Alabi N, Barnes J, et al. 2019. Update: influenza activity—United States, September 30, 2018–February 2, 2019. *Morb. Mortal. Wkly. Rep.* 68:125–34
3. Browne C, Smith R, Bourouiba L. 2015. From regional pulse vaccination to global disease eradication: insights from a mathematical model of poliomyelitis. *J. Math. Biol.* 71:215–53
4. CDC (Cent. Dis. Control Prev.). 2017. *Severe acute respiratory syndrome* (*SARS*). Inf. Sheet, CDC, Washington, DC. **https://www.cdc.gov/sars/index.html**
5. CDC. 2019. *Middle East respiratory syndrome* (*MERS*)—*transmission*. Inf. Sheet, CDC, Washington, DC. **http://www.cdc.gov/coronavirus/mers/about/transmission.html**
6. Shrestha S, Swerdlow D, Borse R, Prabhu V, Finelli L, et al. 2011. Estimating the burden of 2009 pandemic influenza A (H1N1) in the United States (April 2009–April 2010). *Clin. Infect. Dis.* 52:75–82
7. WHO (World Health Organ.). 2018. *Global Health Observatory* (*GHO*) *data—tuberculosis* (*TB*). Inf. Sheet, WHO, Geneva, Switz. **https://www.who.int/gho/tb/en/**
8. Lancet Comm. Tuberc. 2019. Building a tuberculosis-free world. *Lancet* 393:1331–84
9. Nathan C. 2009. Taming tuberculosis: a challenge for science and society. *Cell Host Microbe* 5:220–24
10. CDC. 2017. *Seasonal flu death estimate increases worldwide*. Press Release, CDC, Washington, DC. **https://www.cdc.gov/media/releases/2017/p1213-flu-death-estimate.html**
11. Helmerhorst E, Oppenheim F. 2007. Saliva: a dynamic proteome. *J. Dent. Res.* 86:680–93
12. Schipper R, Silletti E, Vingerhoeds M. 2007. Saliva as research material: biochemical, physicochemical and practical aspects. *Arch. Oral Biol.* 52:1114–35
13. Beeley J. 1993. Fascinating families of proteins: electrophoresis of human saliva. *Biochem. Soc. Trans.* 21:133–38

14. Haward S, Odell J, Berry M, Hall T. 2011. Extensional rheology of human saliva. *Rheol. Acta* 50:869–79
15. Kleinstreuer C, Zhang Z. 2010. Airflow and particle transport in the human respiratory system. *Annu. Rev. Fluid Mech.* 42:301–34
16. Pedley T. 1977. Pulmonary fluid dynamics. *Annu. Rev. Fluid Mech.* 9:229–74
17. Bourouiba L. 2021. The fluid dynamics of disease transmission. *Annu. Rev. Fluid Mech.* 53:473–508
18. Pasteur L. 1861. Mémoire sur les corpuscules organisés qui existent dans l'atmosphère; examen de la doctrine de générations spontanées. *Ann. Sci. Nat.* 16:5–98
19. Koch R. 1876. Untersuchungen über Bakterien. V. Die Aetiologie der Milzbrandkrankheit, begründet auf der Entwicklungsgeschichte des *Bacillus anthracis*. *Beitr. Biol. Pflanz.* 2:277–310
20. SARS Comm. 2006. *SARS Commission Final Report*, Vol. 3: *The Spring of Fear*. Ottawa, Can.: SARS Comm. **http://www.archives.gov.on.ca/en/e_records/sars/report/index.html**
21. Bourouiba L. 2020. Turbulent gas clouds and respiratory pathogen emissions: potential implications for reducing transmission of COVID-19. *JAMA* 323:1837–38
22. Morawska L, Cao J. 2020. Airborne transmission of SARS-CoV-2: The world should face the reality. *Environ. Int.* 139:105730
23. Flügge C. 1897. Ueber die nächsten Aufgaben zur Erforschung der Verbreitungsweise der Phthise. *Dtsch. Med. Wochenschr.* 23:665–68
24. Hirst J. 1995. Bioaerosols: introduction, retrospect and prospect. In *Bioaerosols Handbook*, ed. C Wathes, CS Cox, pp. 5–14. Boca Raton, FL: CRC
25. Flügge C. 1899. Die Verbreitung der Phthise durch staubförmiges Sputum und durch beim Husten verspritzte Tröpfchen. *Z. Hyg. Infekt.* 30:107–24
26. Flügge C. 1905. Ueber Luftverunreinigung, Wärmestauung und Lüftung in geschlossenen Räumen. *Z. Hyg. Infekt.* 49:363–87
27. Flügge C. 1908. *Die Verbreitungsweise und Bekämpfung der Tuberkulose aufgrund experimenteller Untersuchungen im hygienischen Institut der Kgl. Universität Breslau 1897–1908*. Leipzig, Ger.: Veit
28. Flügge C. 1897. Ueber Luftinfection. *Z. Hyg. Infekt.* 25:179–224
29. Laschtschenko P. 1899. Ueber Luftinfektion durch beim Husten, Niessen und Sprechen verspritzte Tröpfchen. *Z. Hyg. Infekt.* 30:125–38
30. Heymann B. 1899. Ueber die Ausstreuung infectiöser Tröpfchen beim Husten der Phthisiker. *Z. Hyg. Infekt.* 30:139–62
31. Ziesché H. 1907. Über die quantitative Verhältnisse der Tröpfchenausbreitung durch hustende Phthisiker. *Z. Hyg. Infekt.* 50:50–82
32. Langmuir A. 1980. Changing concepts of acute contagious diseases: a reconsideration of classic epidemiologic theories. *Ann. N. Y. Acad. Sci.* 353:35–44
33. Wells W. 1955. *Airborne Contagion and Air Hygiene: An Ecological Study of Droplet Infection*. Cambridge, MA: Harvard Univ. Press
34. Verreault D, Moineau S, Duchaine C. 2008. Methods for sampling of airborne viruses. *Microbiol. Mol. Biol. Rev.* 72:413–44
35. Wells W. 1934. On air-born infection. Study II. Droplet and droplet nuclei. *Am. J. Epidemiol.* 20:611–18
36. Hare R. 1964. The transmission of respiratory infections. *Proc. R. Soc. Lond.* 57:221–30
37. Macher J, ed. 1999. *Bioaerosols: Assessment and Control*. Boca Raton, FL: CRC. 3rd ed.
38. Rom W, Garay S. 2017. *Tuberculosis*. Philadelphia: Lippincott, Williams & Wilkins. 2nd ed.
39. Bourouiba L, Dehandschoewercker E, Bush J. 2014. Violent expiratory events: on coughing and sneezing. *J. Fluid Mech.* 745:537–63
40. Bourouiba L. 2016. A sneeze. *N. Engl. J. Med.* 375:e15
41. Jones N, Qureshi Z, Temple R, Larwood J, Greenhalgh T, et al. 2020. Two metres or one: What is the evidence for physical distancing in COVID-19? *BMJ* 370:m3223
42. Abkarian M, Mendez S, Xue N, Yang F, Stone H. 2020. Speech can produce jet-like transport relevant to asymptomatic spreading of virus. *PNAS* 117(41):25237–45
43. Chong K, Ng C, Hori N, Yang R, Verzicco R, et al. 2020. Extended lifetime of respiratory droplets in a turbulent vapour puff and its implications on airborne disease transmission. *Phys. Rev. Lett.* 126:034502
44. Morton BR, Taylor GI, Turner JS. 1956. Turbulent gravitational convection from maintained and instantaneous sources. *Proc. R. Soc. A* 234:1–23

45. Scorer R. 1957. Experiments on convection of isolated masses of buoyant fluid. *J. Fluid Mech.* 2:583–94
46. von Weismayr A. 1898. Zur Frage der Verbreitung der Tuberkulose. *Wien. Klin. Wochenschr.* 46:1039–45
47. Clark R, de Calcina-Goff M. 2009. Some aspects of the airborne transmission of infection. *J. R. Soc. Interface* 6(Suppl. 6):S767–82
48. Richardson L. 1926. Atmospheric diffusion shown on a distance-neighbor graph. *Proc. R. Soc. Lond.* 110:709–37
49. Balachandar S, Zaleski S, Soldati A, Ahmadi G, Bourouiba L. 2020. Host-to-host airborne transmission as a multiphase flow problem for science-based social distance guidelines. *Int. J. Multiphase Flow* 132:103439
50. Okubo A. 1971. Oceanic diffusion diagrams. *Deep-Sea Res.* 18:789–802
51. Bahl P, Bhattacharjee S, de Silva A, Doolan C, MacIntyre C. 2020. Face coverings and mask to minimise droplet dispersion and aerosolisation: a video case study. *Thorax* 75:1024–25
52. Linden P. 1999. The fluid mechanics of natural ventilation. *Annu. Rev. Fluid Mech.* 31:201–38
53. Bhagat R, Davies Wykes M, Dalziel S, Linden P. 2020. Effects of ventilation on the indoor spread of COVID-19. *J. Fluid Mech.* 903:F1
54. ASHRAE Standing Stand. Proj. Com. 2019. *ANSI/ASHRAE Standard 62.1-2019: ventilation for acceptable indoor air quality*. Tech. Rep., Am. Soc. Heat. Refrig. Air-Cond. Eng., Atlanta, GA
55. Tang J, Liebner T, Craven B, Settles G. 2009. A Schlieren optical study of the human cough with and without wearing masks for aerosol infection control. *J. R. Soc. Interface* 6:S727–36
56. Morey P. 1994. Suggested guidance on prevention of microbial contamination for the next revision of ASHRAE Standard 62. In *Proceedings of IAQ'94: Engineering Indoor Environments*, pp. 139–48. Atlanta, GA: Am. Soc. Heat., Refrig. Air-Cond. Eng.
57. Chu D, Akl E, Duda S, Solo K, Yaacoub S, et al. 2020. Physical distancing, face masks, and eye protection to prevent person-to-person transmission of SARS-CoV-2 and COVID-19: a systematic review and meta-analysis. *Lancet* 395:P1973–87
58. Liu W, Tang F, Fang L, De Vlas S, Ma H, et al. 2009. Risk factors for SARS infection among hospital healthcare workers in Beijing: a case control study. *Trop. Med. Int. Health* 14:52–59
59. Offeddu V, Yung C, Low M, Tam C. 2017. Effectiveness of masks and respirators against respiratory infections in healthcare workers: a systematic review and meta-analysis. *Clin. Inf. Dis.* 65:1934–42
60. Wang Y, Tian H, Zhang L, Zhang M, Guo D, et al. 2020. Reduction of secondary transmission of SARS-CoV-2 in households by face mask use, disinfection and social distancing: a cohort study in Beijing, China. *BMJ Glob. Health* 5:e002794
61. Mao N. 2017. Nonwoven fabric filters. In *Fibrous Filter Media*, ed. P Brown, C Cox, pp. 133–71. Cambridge, UK: Woodhead
62. Gao S, Kim J, Yermakov M, Elmashae Y, He X, et al. 2016. Performance of N95 FFRs against combustion and NaCl aerosols in dry and moderately humid air: manikin-based study. *Ann. Occup. Hyg.* 60:748–60
63. Mahdavi A, Haghighat F, Bahloul A, Brochot C, Ostiguy C. 2015. Particle loading time and humidity effects on the efficiency of an N95 filtering facepiece respirator model under constant and inhalation cyclic flows. *Ann. Occup. Hyg.* 59:629–40
64. Ramirez J, O'Shaughnessy P. 2016. The effect of simulated air conditions on N95 filtering facepiece respirators performance. *J. Occup. Environ. Hyg.* 13:491–500
65. Reponen C, McKay R, Haruta H, Sekar P. 2010. Large particle penetration through N95 respirator filters and facepiece leaks with cyclic flow. *Ann. Occup. Hyg.* 54:68–77
66. Rengasamy S, Eimer B, Shaffer R. 2010. Simple respiratory protection—evaluation of the filtration performance of cloth masks and common fabric materials against 20–1000 nm size particles. *Ann. Occup. Hyg.* 54:789–98
67. Konda A, Prakash A, Moss G, Schmoldt G, Guha S. 2020. Aerosol filtration efficiency of common fabrics used in respiratory cloth masks. *ACS Nano* 14:6339–47
68. Deleted in proof
69. Chao C, Wan M, Morawska L, Johnson G, Ristovski Z, et al. 2009. Characterization of expiration air jets and droplet size distributions immediately at the mouth opening. *Aerosol Sci.* 40:122–33
70. Han Z, Weng W, Huang Q. 2013. Characterizations of particle size distribution of the droplets exhaled by sneeze. *J. R. Soc.* 10:20130560

71. Deleted in proof
72. Deleted in proof
73. Zayas G, Chiang M, Wong E, MacDonald F, Lange C, et al. 2012. Cough aerosol in healthy participants: fundamental knowledge to optimize droplet-spread infectious respiratory disease management. *BMC Pulm. Med.* 12:11
74. Lee J, Yoo D, Ryu S, Ham S, Lee K, et al. 2019. Quantity, size distribution, and characteristics of cough-generated aerosol produced by patients with an upper respiratory tract infection. *Aerosol Air Qual. Res.* 19:840–53
75. Yang S, Lee GWM, Chen CM, Wu CC, Yu KP. 2007. The size and concentration of droplets generated by coughing in human subjects. *J. Aerosol Med.* 20:484–94
76. Asadi S, Wexler A, Cappa C, Barreda S, Bouvier N, et al. 2019. Aerosol emission and superemission during human speech increases with voice loudness. *Sci. Rep.* 9:2348
77. Morawska L, Johnson GR, Ristovski ZD, Hargreaves M, Mengersen K, et al. 2009. Size distribution and sites of origin of droplets expelled from the human respiratory tract during expiratory activities. *J. Aerosol Sci.* 40:256–69
78. Duguid J. 1945. The numbers and the sites of origin of the droplets expelled during expiratory activities. *Edinb. Med. J.* 52:385–401
79. Johnson G, Morawska L, Ristovski Z, Hargreaves M, Mengersen K, et al. 2011. Modality of human expired aerosol size distributions. *J. Aerosol Sci.* 42:839–51
80. Deleted in proof
81. Cheng Y, Wang C, You S, Hsieh N, Chen W, et al. 2016. Assessing coughing-induced influenza droplet transmission and implications for infection risk control. *Epidemiol. Infect.* 144:333–45
82. Deleted in proof
83. Fabian P, McDevitt J, DeHaan W, Fung R, Cowling B, et al. 2008. Influenza virus in human exhaled breath: an observational study. *PLOS ONE* 3:e2691
84. Holmgren H, Gerth E, Ljungström E, Larsson P, Almstrand A, et al. 2013. Effects of breath holding at low and high lung volumes on amount of exhaled particles. *Respir. Physiol. Neurobiol.* 185:228–34
85. Lindsley W, Pearce T, Hudnall J, Davis K, Davis S, et al. 2012. Quantity and size distribution of cough-generated aerosol particles produced by influenza patients during and after illness. *J. Occup. Environ. Hyg.* 9:443–49
86. Papineni RS, Rosenthal FS. 1997. The size distribution of droplets in the exhaled breath of healthy human subjects. *J. Aerosol Med.* 10:105–16
87. Deleted in proof
88. Deleted in proof
89. Gerone P, Couch R, Keefer G, Douglas R, Derrenbacher E, et al. 1966. Assessment of experimental and natural viral aerosols. *Bacteriol. Rev.* 30:576–84
90. Hersen G, Moularat S, Robine E, Gehin E, Corbet S, et al. 2008. Impact of health on particle size of exhaled respiratory aerosols: case-control study. *Clean* 36:572–77
91. Loudon R, Roberts R. 1967. Droplet expulsion from the respiratory tract. *Am. Rev. Respir. Dis.* 95:435–42
92. Johnson G, Morawska L, Ristovski Z, Hargreaves M, Mengersen K, et al. 2011. Modality of human expired aerosol size distributions. *J. Aerosol Sci.* 42:839–51
93. Xie X, Li Y, Sun H, Liu L. 2009. Exhaled droplets due to talking and coughing. *J. R. Soc. Interface* 6(Suppl. 6):S703–14
94. Baron P, Willeke K. 2001. *Aerosol Measurement: Principles, Techniques, and Applications*. New York: Wiley. 2nd ed.
95. Black D, McQuay M, Bonin M. 1996. Laser-based techniques for particle-size measurement: a review of sizing methods and their industrial applications. *Prog. Energy Combust. Sci.* 22:267–306
96. TSI. 2012. *Aerodynamic Particle Sizer model 3321: theory of operation*. Publ. P/N 5001469 Rev. A, TSI, Shoreview, MN. **https://www.tsi.com/getmedia/26cd9e57-9050-4a57-a442-3ec3a4338808/3321%20Operation%20brochure%20A4-5001469_WEB?ext=.pdf**
97. Alsved M, Bourouiba L, Duchaine C, Löndahl J, Marr L, et al. 2020. Natural sources and experimental generation of bioaerosols: challenges and perspectives. *Aerosol Sci. Technol.* 54:547–71

98. Zanin M, Baviskar P, Webster R, Webby R. 2016. The interaction between respiratory pathogens and mucus. *Cell Host Microbe* 19:159–68
99. Ruhl C, Pasko B, Khan H, Kindt L, Stamm C, et al. 2020. *Mycobacterium tuberculosis* sulfolipid-1 activates nociceptive neurons and induces cough. *Cell* 181:293–305.e11
100. Rubin B. 2010. The role of mucus in cough research. *Lung* 188:69–72
101. Villermaux E. 2007. Fragmentation. *Annu. Rev. Fluid Mech.* 39:419–46
102. Villermaux E. 2020. Fragmentation versus cohesion. *J. Fluid Mech.* 898:P1
103. Eggers J, Villermaux E. 2008. Physics of liquid jets. *Rep. Prog. Phys.* 71:036601
104. Lefebvre AH, McDonell VG. 2017. *Atomization and Sprays*. Boca Raton, FL: CRC. 2nd ed.
105. Bourouiba L. 2013. Understanding the transmission of H5N1. *CAB Rev.* 8:1–8
106. Grotberg JB. 2001. Respiratory fluid mechanics and transport processes. *Annu. Rev. Biomed. Eng.* 3:421–57
107. Wang Y, Bourouiba L. 2018. Non-isolated drop impact on surfaces. *J. Fluid Mech.* 835:24–44
108. Wang Y, Bourouiba L. 2018. Unsteady sheet fragmentation: droplet sizes and speeds. *J. Fluid Mech.* 848:946–67
109. Scharfman BE, Techet AH, Bush JWM, Bourouiba L. 2016. Visualization of sneeze ejecta: steps of fluid fragmentation leading to respiratory droplets. *Exp. Fluids* 57:24
110. Déchelette A, Babinsky E, Sojka PE. 2011. Drop size distributions. See Ref. 123, pp. 479–95
111. Clanet C, Villermaux E. 2002. Life of a smooth liquid sheet. *J. Fluid Mech.* 462:307–40
112. Bremond N, Villermaux E. 2006. Atomization by jet impact. *J. Fluid Mech.* 549:273–306
113. Wang Y, Bourouiba L. 2017. Drop impact on small surfaces: thickness and velocity profiles of the expanding sheet in the air. *J. Fluid Mech.* 814:510–34
114. Walls P, Bird J, Bourouiba L. 2014. Moving with bubbles: a review of the interactions between bubbles and the microorganisms that surround them. *Integr. Comp. Biol.* 54:1014–25
115. Poulain S, Villermaux E, Bourouiba L. 2018. Aging and burst of surface bubbles. *J. Fluid Mech.* 851:636–71
116. Scharfman B, Techet A. 2012. Bag instabilities. *Phys. Fluids* 24:091112
117. Bourouiba L, Bush JWM. 2013. Drops and bubbles in the environment. In *Handbook of Environmental Fluid Dynamics*, Vol. 1: *Overview and Fundamentals*, ed. HJ Fernando, pp. 427–39. Boca Raton, FL: CRC
118. Poulain S, Bourouiba L. 2018. Biosurfactants change the thinning of contaminated bubbles at bacteria-laden water interfaces. *Phys. Rev. Lett.* 121:204502
119. Néel B, Villermaux E. 2018. The spontaneous puncture of thick liquid films. *J. Fluid Mech.* 838:192–221
120. Culick F. 1960. Comments on a ruptured soap film. *J. Appl. Phys.* 31:1128–29
121. Clasen C, Eggers J, Fontelos M, Li J, McKinley G. 2006. The beads-on-string structure of viscoelastic threads. *J. Fluid Mech.* 556:283–308
122. Wagner C, Bourouiba L, McKinley G. 2015. An analytic solution for capillary thinning and breakup of FENE-P fluids. *J. Non-Newton. Fluid Mech.* 218:53–61
123. Ashgriz N, ed. 2011. *Handbook of Atomization: Theory and Application*. New York: Springer
124. Wang Y, Bourouiba L. 2021. Growth and breakup of ligaments in unsteady fragmentation. *J. Fluid Mech.* 910:A39
125. Wang Y, Dandekar R, Bustos N, Poulain S, Bourouiba L. 2018. Universal rim thickness in unsteady sheet fragmentation. *Phys. Rev. Lett.* 120:204503
126. Ouyang W, Han J. 2019. Universal amplification-free molecular diagnostics by billion-fold hierarchical nanofluidic concentration. *PNAS* 116:16240–49
127. Mbareche H, Veillette M, Teertstra W, Kegel W, Bilodeau G, et al. 2019. Recovery of fungal cells from air samples: a tale of loss and gain. *Appl. Environ. Microbiol.* 85:e02941
128. van Doremalen N, Bushmaker T, Morris D, Holbrook M, Gamble A, et al. 2020. Aerosol and surface stability of SARS-CoV-2 as compared with SARS-CoV-1. *N. Engl. J. Med.* 382:1564–67
129. Bean B, Moore B, Sterner B, Peterson L, Gerding D, et al. 1982. Survival of influenza viruses on environmental surfaces. *J. Infect. Dis.* 146:47–51
130. Hall C. 2007. The spread of influenza and other respiratory viruses: complexities and conjectures. *Clin. Infect. Dis.* 45:353–59

131. Bloch A, Orenstein W, Ewing W, Spain W, Mallison G, et al. 1985. Measles outbreak in a pediatric practice: airborne transmission in an office setting. *Pediatrics* 75:676–83
132. Remington P, Hall W, Davis I, Herald A, Gunn R. 1985. Airborne transmission of measles in a physician's office. *JAMA* 253:1574–77
133. Loudon R, Bumgarner L, Lacy J, Coffman G. 1969. Aerial transmission of mycobacteria. *Am. Rev. Respir. Dis.* 100:165–71
134. Kormuth KA, Lin K, Prussin A, Vejerano EP, Tiwari AJ, et al. 2018. Influenza virus infectivity is retained in aerosols and droplets independent of relative humidity. *J. Infect. Dis.* 218:739–47
135. Smither S, Eastaugh L, Findlay J, Lever M. 2020. Experimental aerosol survival of SARS-CoV-2 in artificial saliva and tissue culture media at medium and high humidity. *Emerg. Microbes Infect.* 9:1415–17
136. Fears AC, Klimstra WB, Duprex P, Hartman A, Weaver SC, et al. 2020. Comparative dynamic aerosol efficiencies of three emergent coronaviruses and the unusual persistence of SARS-CoV-2 in aerosol suspensions. medRxiv 20063784. **https://doi.org/10.1101/2020.04.13.20063784**
137. Chin A, Chu J, Perera M, Hui K, Yen HL, et al. 2020. Stability of SARS-CoV-2 in different environmental conditions. *Lancet Microbe* 1:e10
138. Matson M, Yinda C, Seifert S, Bushmaker T, Fischer R, et al. 2020. Effect of environmental conditions on SARS-CoV-2 stability in human nasal mucus and sputum. *Emerg. Infect. Dis.* 26:2276–78
139. Riddell S, Goldie S, Hill A, Eagles D, Drew T. 2020. The effect of temperature on persistence of SARS-CoV-2 on common surfaces. *Virol. J.* 17:145
140. Chan KH, Sridhar S, Zhang R, Chu H, Fung AYF, et al. 2020. Factors affecting stability and infectivity of SARS-CoV-2. *J. Hosp. Infect.* 106:226–31
141. Sonkin LS. 1951. The role of particle size in experimental airborne infection. *Am. J. Hyg.* 53:337–54
142. Majumder MS, Brownstein JS, Finkelstein SN, Larson RC, Bourouiba L. 2017. Nosocomial amplification of MERS-coronavirus in South Korea, 2015. *Trans. R. Soc. Trop. Med. Hyg.* 111:261–69
143. Levy S, Alladina J, Hibbert K, Harris R, Bajwa E, et al. 2016. High-flow oxygen therapy and other inhaled therapies in intensive care units. *Lancet* 387:1867–78

Annual Review of Biomedical Engineering

Volume 23, 2021

Contents

Errata

An online log of corrections to *Annual Review of Biomedical Engineering* articles may be found at http://www.annualreviews.org/errata/bioeng